CANADIAN CLIMATE CENTRE

REPORT NO. 89-10

# EVALUATION OF STATE-OF-THE-ART DRILLING PLATFORM ICING MODELS

by

R.D. Brown
and
I. Horjen

ATMOSPHERIC ENVIRONMENT SERVICE

DOWNSVIEW, ONTARIO

1989

THIS REPORT HAS RECEIVED ONLY LIMITED CIRCULATION BECAUSE OF THE SPECIAL NATURE OF THE PROJECT. HOWEVER, REFERENCE IS PERMITTED IF THE WORDS "UNPUBLISHED MANUSCRIPT" ARE MADE PART OF THE BIBLIOGRAPHIC ENTRY, IN ACCORDANCE WITH ACCEPTED PRACTICE.

**OTHER CANADIAN CLIMATE CENTRE (CCC)**
**SCIENTIFIC SERIES INCLUDE:**

1. CS series - CCC Climatological Study
2. CLI series - CCC Climatological Memoranda
3. CDS/DS series - CCC Climatic Data Summary
   - CCC Documentation Sheet

For further information on climatological publications contact the

Climatological Services Division
Atmospheric Environment Service
4905 Dufferin Street
Downsview, Ontario M3H 5T4

# EVALUATION OF STATE-OF-THE-ART DRILLING PLATFORM ICING MODELS

by

R.D. Brown[1]
and
I. Horjen[2]

[1]Atmospheric Environment Service
[2]Norwegian Hydrotechnical Laboratory

This work was supported by the Federal Panel on Energy R&D

**A publication of the Canadian Climate Program**

## ABSTRACT

This report describes the results of a joint evaluation of two state-of-the-art drilling platform icing models: ICEMOD, a fully time-dependent model developed by the Norwegian Hydrotechnical Laboratory (NHL), and RIGICE, a stationary icing model developed for the Canadian Atmospheric Environment Service (AES). The evaluation of ICEMOD and RIGICE was carried out at three levels: sensitivity analysis, wind tunnel experiments, and comparisons with data from 7 documented platform icing events.

The sensitivity analysis showed both models to have essentially the same response to variation in the main icing variables for the warmer air and sea-surface temperatures typically encountered during icing events in the North Sea. For the colder air and sea-surface temperatures typical of Canadian east coast icing events, however, RIGICE exhibited much greater sensitivity to variation in sea-surface temperature, salinity and air temperature. The main reasons for the different stationary model response were considered to be related to a constant $\dot{Q}_w$ and the lack of the time-dependent feedback mechanism of increasing brine film salinity.

The wind tunnel experiments demonstrated the superior performance of the time-dependent model for pulsed, saline spray conditions. A curvilinear relationship was found between the peak liquid water content implementation of RIGICE and ICEMOD, which initially suggested it may be possible to "calibrate" stationary models to include time-dependent effects. However, it was later concluded that such calibration was not feasible because the experimental conditions were not typical of icing conditions experienced offshore.

Comparisons of model performance for a number of documented drilling platform icing cases showed that both models were able to provide realistic estimates of ice accretion thicknesses and ice loads for warmer water, lower wave height icing events. The inclusion of simple sheltering assumptions in RIGICE produced ice loads which were very close to those predicted by ICEMOD. However,

both models were found to considerably overpredict ice accretion amounts for three icing events with cold sea-surface temperatures and higher wave conditions.

More detailed conclusions about model performance will require quantitative icing field data. These initial findings suggest that further enhancements to both models are required to provide reliable ice loads on offshore structures over a wide range of environmental conditions. In particular, an effort needs to be made to develop and test a physically-based spraying model for offshore structures, along with quantitative documentation of the nature and magnitude of the time-dependencies in saline, pulsed spray icing under conditions which closely simulate the marine environment.

## RÉSUMÉ

Ce rapport présente les résultats de l'évaluation comparative de deux modèles sophistiqués de givrage des plates-formes de forage: le modèle ICEMOD, modèle temporel créé par le laboratoire hrdrotechnique de Norvège, et le modèle RIGICE, modèle statique de givrage créé pour le Service de l'environnement atmosphérique du Canada (SEA). Ces deux modèles ont été évalués sous trois angles: analyse de sensibilité, expérience en soufflerie et comparaison aves les données provenant de sept cas de givrage de plate-forme.

L'analyse de sensibilité a montré que les deux modèles répondaient essentiellement de la même façon aux variations des principales variables intervenant dan le phénomème de givrage pour des températures de l'air et de surface de la mer relativement chaudes typiques de la mer du Nord. Par contre quand les températures de l'air et de la surface de la mer sont plus froides, comme c'est le cas sur la côte est du Canada, le modèle RIGICE est beaucoup plus sensibles aux variations de la salinité et des températures de l'eau et de l'air. La constance du paramètre $\dot{Q}_w$ et l'absence d'un mécanisme de rétroaction temporel relatif à l'augmentation de la salinité du film d'eau saumâtre seraient les deux principaux facteurs expliquant le fait que le modèle statique a donné une réponse différente.

Par ailleur, le modèle temporel s'est avéré supérieur au cours d'expériences menées en soufflerie dans lesquelles des embruns salins sont projetés rythmiquement sur les structures. Il existe une relation curvilinéaire entre les contenus maximums de l'air en eau liquide déterminés par les modèles RIGICE et ICEMOD, ce qui nous a d'abord fait penser qu'il pouvait être possible d'"étalonner" les modèles statiques de façon à ce qu'ils puissent prendre en compte les facteurs temporels. Cependent, nous nous sommes aperçus par la suite qu'un tel étalonnage était impossible à réaliser parce que les conditions expérimentales dans lesquelles il pouvait être réalisé ne correspondaient pas aux conditions de givrage rencontrées en mer.

D'après la comparaison des résultats des modèles aves les données disponibles sur le givrage des plates-formes, les deux modèles se sont montrés aptes à donner des estimations réalistes des épaisseurs et des quantités de verglas accumulées sur les structures quand les eaux sont relativement chaudes et les vagues relativement basses. En introduisant dans le modèle RIGICE des hypothèses simples relatives au fait que certaines parties de la structures des plates-formes sont abritées, nous avons obtenu des résultats presque identiques à ceux du modèle ICEMOD en ce qui a trait à la quantité de verglas accumulé. Cependent, les deux modèles ont considérablement surévalué les quantités de verglas accumulé dans trois cas où les températures de la surface de la mer étaient froides et les vagues, hautes.

Nous avons besoin de données empiriques quantitatives sur le givrage pour évaluer de façon plus détaillée la valeur de ces modèles. Ces premiers résultats montrent que des améliorations devront être apportées à chacun de ces modèles si l'on veut obtenir des estimations fiables des quantités de verglas accumulé sur les structure en mer dans des conditions environnementales très variées. En particulier, il faudra élaborer et tester un modèle fondé sur des critères physiques pour les embruns, modèles applicables aux structures situées en mer, et obtenir des données quantitative relatives à la nature et à l'ampleur des facteurs temporels intervenants dans le givrage dû à des embruns salés dans des conditions simulant de près celles du milieu marin.

## ACKNOWLEDGEMENTS

The authors wish to acknowledge a number of inividuals and organizations who contributed to this study. Many thanks to David Minsk (formerly of CRREL) for supplyimg the SEDCO 708 icing data, and to Jon Nauman of the U.S. Minerals Management Service for the OCEAN BOUNTY data. Thanks are also extended to Paul Mitten of Compusult Limited for supplying numerous pieces of required information, and to the Rowan Drilling Company and ODECO for supplying the drilling platform dimensions needed in the icing simulations. This study would not have been possible without the cooperation of the oil companies and operators involved in the platform icing cases investigated. These include Petro-Canada, Shell, Husky Bow Valley, Phillips Petroleum and ARCO Alaska. Tore Jørgensen of NHL is acknowledged for his critical role in getting the Norwegian side of the project funded. Funding for the study was provided by the Canadian Federal Panel on Energy Research and Development (PERD), and the Royal Norwegian Council of Scientific and Industrial Research.

Table of Contents:


| | page |
|---|---|
| ABSTRACT | i |
| RÉSUMÉ | iii |
| ACKNOWLEDGEMENTS | v |
| 1.0 INTRODUCTION | 1 |
| 2.0 ICEMOD | 2 |
| 2.1 The basic icing equations | 7 |
| 2.2 Initial conditions | 11 |
| 2.3 Icing for selected geometries | 11 |
| 2.3.1 Horizontal cylinder and plate | 12 |
| 2.3.2 Vertical plate | 13 |
| 2.3.3 Vertical cylinder | 14 |
| 2.4 Impinging spray flux | 17 |
| 2.5 Model configuration | 18 |
| 3.0 RIGICE | 20 |
| 3.1 Theoretical background | 22 |
| 3.1.1 Impinging spray flux | 23 |
| 3.1.2 Heat transfer | 23 |
| 3.1.3 Heat balance | 25 |
| 3.2 Model configuration | 27 |
| 4.0 MODEL EVALUATION | 28 |
| 4.1 Sensitivity analysis | 29 |
| 4.1.1 North Sea condition | 30 |
| 4.1.2 East Coast condition | 35 |
| 4.2 Wind tunnel simulations | 40 |
| 4.2.1 Experimental conditions | 40 |
| 4.2.2 Results | 42 |
| 4.3 Drilling platform icing cases | 44 |
| 4.3.1 Ice thickness profiles | 59 |
| 4.3.2 Ice thickness observations | 62 |
| 4.3.3 Ice mass estimates | 64 |
| 5.0 CONCLUSIONS | 68 |
| 6.0 RECOMMENDATIONS | 69 |
| 7.0 REFERENCES | 71 |
| APPENDIX A: Heat exchange relationships used in ICEMOD for the brine film. | 75 |

## 1.0 INTRODUCTION

Ice accretion from freezing spray is a frequent winter marine hazard off the east coast of Canada and in the Barents Sea (Brown and Mitten, 1988; Jørgensen, 1982). However, there is little quantitative icing information available for estimating ice loading norms and extremes. The Norwegian offshore petroleum industry approached this problem in the early 1980's by sponsoring a marine icing research program at the Norwegian Hydrotechnical Laboratory (NHL) to develop techniques for modelling ice loads and the heat requirements for anti- and de-icing purposes. The "Offshore Icing" program which commenced in 1983 involved three main components: (1) collection of field data on the sea spray generation characteristics of semi-submersibles and supply vessels, (2) construction of a wind tunnel for controlled spray icing experiments, and (3) development of a comprehensive numerical model for predicting ice accretion on offshore structures and vessels. The research culminated in 1986 with the development of the stationary numerical icing model ICEMOD (Horjen and Vefsnmo, 1986a). In 1987 the project was extended by operators north of 62°N to incorporate time-dependent effects from local changes in brine film temperature, salinity and thickness into ICEMOD (Horjen and Vefsnmo, 1987). More recently, ICEMOD has been enhanced to include the effects of wind and spray stress on brine film movement over an icing surface (Horjen et al. 1988).

The situation is somewhat different in Canada where winter drilling has been largely confined to the Scotian Shelf and Grand Banks areas since the early 1970's. From experience gained over this period, Canadian operators concluded that spray icing produced very small amounts of ice on drilling platforms, and was rarely an operational problem (Brown and Roebber, 1985). Government regulatory agencies, however, were less willing to dismiss icing as non-consequential for a number of reasons. First, there was documented evidence of a severe icing event on the SEDNETH I which nearly resulted in the jettison of drilling fluids and drill pipe (Agnew, 1985). Second, the icing experience of east coast operators was temporally and spatially constrained. And

third, there were no reliable estimates available of extreme ice loads on offshore structures. This latter knowledge gap together with the fact that NHL's icing model was proprietary, prompted the Canadian Atmospheric Environment Service (AES) to initiate a contract in 1986 to develop an icing model suitable for predicting ice accretion thicknesses and loadings on offshore structures. A stationary icing model, RIGICE, was completed in early 1987 by The MEP Company together with Drs. E.P. Lozowski and L. Makkonen (Roebber and Mitten, 1987).

During initial attempts to verify RIGICE with field data, it became apparent from discussions between NHL and AES that both organizations were independently pursuing the same objective of evaluating model performance. This set the stage for a cooperative model evaluation project involving exchange of icing data, scientists and expertise. The following sections describe the results of this cooperative project: Sections 2.0 and 3.0 describe the two models being evaluated, Section 4.0 presents the evaluation methodology, data and results, while a summary and conclusions is given in Section 5.0.

## 2.0 ICEMOD

In the early 1980's, the Norwegian offshore petroleum industry was making preparations to expand exploration to higher latitudes off northern Norway and in the Barents Sea. It was recognized that sea spray icing in these environments could adversely affect safety and marine operations. A comprehensive marine icing research effort was therefore established at the Norwegian Hydrotechnical Laboratory in 1983, sponsored by the oil companies with licenses at Troms I. The major goal of the research program was to develop techniques for predicting (1) ice loads on offshore structures and supply vessels, and (2) the heat requirements for anti- and de-icing these structures and vessels.

A key element of the research program was the collection of field data on the characteristics of spray generated by wave-structure and wave-vessel impacts e.g. spray frequency, spray fluxes and droplet size distributions (Jørgensen et al., 1986). These data

are crucial for realistic prediction of ice loads from freezing spray. In 1986, the knowledge gained from the field programs culminated in the development of the stationary numerical icing model "ICEMOD" which calculated the icing intensity and the energy necessary for melting accreted ice (de-icing) and for keeping a surface ice free (anti-icing) (Horjen and Vefsnmo, 1986a).

Earlier in 1985, Horjen and Vefsnmo (1985b) had shown that movement of the brine film covering the icing surface had a significant effect on the icing intensity. In 1987, research was therefore sponsored by Norwegian operators north of 62°N to include effects arising from spatial and temporal variation of brine film enthalpy into ICEMOD. The following discussion refers to this time-dependent version of ICEMOD as outlined in Vefsnmo et al. (1987).

NOMENCLATURE FOR ICEMOD:

$C$ = specific heat capacity at constant pressure (J/kg °C)

$k$ = thermal conductivity (W/m °C)

$\dot{Q}$ = unit heat flux ($W/m^2$)

$h$ = ice thickness normal to the phase interface (m)

$t$ = time (s)

$t_s$ = duration of one spray (s)

$p$ = air pressure (kPa)

$f$ = relative humidity (absolute value)

$U_o$ = free stream air velocity (m/s)

$U$ = local wind velocity above the air boundary layer (m/s)

$e$ = saturation vapour pressure over pure water (kPa)

$S$ = salinity (parts per thousand)

$s, n, z$ = orthogonal curvilinear coordinate system fixed to the icing surface with n-direction normal to the surface

$\vec{e}_i$ = unit vector in i-direction

$\vec{v}$ = (u, v, w) velocity vector with components in the s, n, and z-directions (m/s)

$\vec{V}_{sp}$ = $(U_{sp}, V_{sp})$ spray bulk velocity vector upon impact in an absolute reference system with components in the s and n-directions (m/s)

$\overline{Nu}$ = Nusselt number

$L$ = characteristic length (m)

$Pr$ = Prandtl number

$Re$ = Reynolds number

$l_o$ = specific latent heat of fusion of pure ice (J/kg)

$l_f$ = specific latent heat of fusion of saline ice (J/kg)

$l_e$ = specific latent heat of evaporation (J/kg)

$D$ = cylinder diameter (m)

$D_e$ = "effective" cylinder diameter (m) defined in eqn. (2.22)

$M$ = ice weight (kg)

$g$ = acceleration of free fall $\approx 9.81$ m/s$^2$ (50°N)

$G$ = average free stream mass flux of spray per unit area ($kg/m^2s$)

$R_w$ = local water catch rate of impinging spray ($kg/m^2s$)

$C_f$ = local friction coefficient

$X, Y$ = dependent variables in the icing equations defined in Section 2.1 ($kg/m^2$)

$R$ = local icing intensity ($kg/m^2s$)

$\dot{m}$ = mass transfer rate ($kg/m^2s$)

$n$ = freezing fraction ($= R/R_w$)

$N$ = spray frequency ($s^{-1}$)

$H$ = wave height (m)

$T$ = wave period or icing period (s)

GREEK LETTERS

$\theta$ = temperature ($^\circ C$)

$\rho$ = density ($kg/m^3$)

$\beta$ = heat transfer coefficient ($W/m^2\ ^\circ C$)

$\gamma$ = local collection efficiency

$\upsilon$ = kinematic viscosity ($m^2/s$)

$\mu$ = dynamic viscosity ($kg/ms$)

$\kappa$ = thermal diffusivity ($m^2/s$)

$\delta$ = brine film thickness in the n-direction (m)

$\varphi$ = angle defined in Figure 2.1

$\sigma$ = interfacial distribution coefficient

$\lambda$ = convective mass transfer coefficient (m/s)

$\chi$ = mass diffusivity ($m^2/s$)

$\tau$ = total shear stress ($kg/ms^2$)

$\nabla_t$ = gradient operator in the tangential direction
$= \vec{e}_s \frac{\partial}{\partial s} + \vec{e}_z \frac{\partial}{\partial z}$

SUBSCRIPTS

a = air

b = brine film mean value in the normal direction

s = brine/air interface, s-component or significant wave

i = ice

t = tangential direction or total

n = normal direction

v = vapour

(s, z) = vector components along the icing surface

0 = free flow, stagnation point or fresh water

sp = spray

w = spray water

$_{e}$ = evaporation

$_{1}$ = first spray

$_{r}$ = relative

$_{10}$ = 10 m above mean sea level

## THEORETICAL BACKGROUND OF "ICEMOD"

### 2.1 The basic icing equations:

The time-dependent version of ICEMOD is based on the equations of conservation of mass, heat energy and salt content in the brine film covering the ice surface layer during "wet growth". They have the following form (Horjen and Vefsnmo, 1986b):

$$L(X) = R_w + \dot{m}_e - R \tag{2.1}$$

$$C_b X \frac{D\theta_b}{dt} = \dot{Q}_s + l_f R + \dot{Q}_l \tag{2.2}$$

$$X \frac{DS_b}{dt} = R_w S_w - S_b[R_w + \dot{m}_e - R(1-\sigma)] \tag{2.3}$$

where

$$(\ )_b = \frac{1}{\delta}\int_0^{\delta} (\ )\, dn \quad \text{(mean value across the brine film)}$$

and

$$\frac{D(\ )}{dt} = \frac{\partial(\ )}{\partial t} + \vec{v}_b \cdot \nabla_t (\ )$$

$$L(\ ) = \frac{\partial(\ )}{\partial t} + \nabla_t \cdot [(\ )\vec{v}_b]$$

$\nabla_t$ = gradient operator in the tangential direction

$X = \rho_b \delta$

$\sigma = S_i / S_b$ (interfacial distribution coefficient)

The operator L has the property:

$$L(\varphi\,\psi) = \varphi\,L(\psi) + \frac{D\varphi}{dt}\,\psi$$

$\dot{Q}_s$ is the net heat flux at the air/liquid film interface and consists of several terms:

$$\dot{Q}_s = \dot{Q}_c + \dot{Q}_e + \dot{Q}_w + \dot{Q}_r + \dot{Q}_v \qquad (2.4)$$

where

$\dot{Q}_c$ = conduction (sensible) heat flux (convective transport outside the boundary layer)

$\dot{Q}_e$ = evaporative heat flux

$\dot{Q}_w$ = heat transfer between impinging spray and liquid film

$\dot{Q}_r$ = heat transfer by radiation

$\dot{Q}_v$ = heating due to adiabatic compression of air and viscous work in the air boundary layer

$\dot{Q}_i$, the heat flux through the ice is neglected. The heat fluxes are defined negative when the heat transfer is away from the brine film. During sea spray icing $\dot{Q}_i$, $\dot{Q}_c$, $\dot{Q}_e$ and $\dot{Q}_r$ are normally negative while $\dot{Q}_w$ and $\dot{Q}_v$ are positive. A more detailed discussion is given in Appendix A. The term $\dot{m}_e$ in eqns. (2.1) and (2.3) is the mass exchange per unit area (negative) due to evaporation and is given by:

$$\dot{m}_e = \dot{Q}_e / l_e = \frac{0.622\beta}{Le\ C_{a\,p}} [f\ e(\theta_a) - e_b(\theta_b, S_b)] \quad (kg/m^2 s) \qquad (2.5)$$

where Le is the Lewis number defined by:

$$Le = \frac{\beta}{\rho_a\ C_a\ \lambda_a} \approx \left(\frac{\kappa_a}{\chi_v}\right)^{2/3} \approx 0.90$$

The saturation vapour pressure on the surface of the brine film, $e_b$, is lower than its value on a pure water surface at the same temperature. The following relationship was obtained from Witting (1908):

$$e_b(\theta_b, S_b) = (1 - 5.37 \cdot 10^{-4} S_b)\, e(\theta_b) \qquad (2.6)$$

Also, the latent heat of freezing of saline water is lower than the pure water value:

$$l_f = (1 - \sigma)\, l_0 \qquad (2.7)$$

$\sigma$ is equal to the liquid water fraction in the ice layer close to the icing surface, which in the model is assumed to be independent of icing conditions. For saline spray, a mean value for $\sigma$ of 0.34 was obtained from Japanese field data, and Finnish and Russian wind tunnel data (Vefsnmo et al., 1987). When the model is used for fresh water icing, $\sigma$ is set to 0.28 which is the mean value obtained from experiments carried out in the University of Alberta wind tunnel (Gates et al., 1986).

When ice and brine coexist, the composition of the brine is a function of temperature only. The brine salinity can then be obtained from the sea-ice phase equilibrium tables of Assur (1958). Cox and Weeks (1986) have fitted these data to a third-degree polynomial in temperature:

$$S_b = \sum_{i=0}^{3} \alpha_i\, \theta_b^{\,i} \qquad (2.8)$$

where the set of coefficients, $\alpha_i$, depend on the temperature range.

Using this relationship, eqns. (2.2) and (2.3) can be combined to obtain an algebraic expression of the local icing intensity, R:

$$R = \frac{\theta_0\, C_b\, [(S_b - S_w) R_w + \dot{m}_e S_b] - (\dot{Q}_s + \dot{Q}_i)}{(1 - \sigma)\cdot [\theta_0\, C_b\, S_b + l_0]} \qquad (2.9)$$

where

$$\theta_0 = -(\alpha_1 + 2\,\alpha_2 \theta_b + 3\,\alpha_3 \theta_b^{\,2})^{-1}$$

Combining eqns. (2.1) and (2.3) gives:

$$L(Y) = R_w S_w - \sigma R S_b \tag{2.10}$$

where $Y = S_b X$

Eqns. (2.1) and (2.10) are termed the "icing equations". Together with the momentum equation of the brine film, they represent a closed set of non-linear partial differential equations with four dependent variables X, Y, $U_b$ and $W_b$. From the solution of this set of equations, the icing intensity is readily found from eqn. (2.9) as a function of $S_b = Y/X$. Another useful relation is obtained from multiplying eqn. (2.1) by $(S_b - S_w)$ and using the property of the L-operator in eqn. (2.3):

$$L\,[(S_b - S_w)X\,] = R\,(S_w - \sigma S_b) - \dot{m}_e S_w \tag{2.11}$$

Although this relation was derived assuming $X \neq 0$, it is also valid for $X = 0$ provided $R_w = R - \dot{m}_e$, i.e. icing is in the "dry growth" regime.

From eqn. (2.11) it can be readily shown that phase transition at the brine film boundaries (water/ice and water/vapour) results in a brine film salinity different from the spray salinity. For the special case of dry growth:

$$R = R_w + \dot{m}_e \qquad \text{(definition)} \tag{2.12}$$

$$S_b = \frac{R_w S_w}{\sigma\,(R_w + \dot{m}_e)} \gtrsim \frac{S_w}{\sigma} \tag{2.13}$$

In the case of continuous spray, the icing equations may be reduced to a set of ordinary differential equations. Introducing

$$X' = \rho_b \delta v_b$$

$$Y' = S_b X'$$

the equations now transform to

$$\frac{dX'}{ds'} = R_w + \dot{m}_e - R(S_b) \tag{2.14}$$

$$\frac{dY'}{ds'} = R_w S_w - \sigma R S_b \tag{2.15}$$

where s is the coordinate direction of $\vec{v}_b$.

## 2.2 Initial conditions

For all times $t < 0$, it is assumed that a thin layer of ice exists, but there is no spray. At time $t = 0$, the first spray hits the ice surface. The initial condition is then:

$$X = 0, \quad Y = 0, \quad \vec{v}_b = \vec{0} \quad \text{for} \quad t = 0 \tag{2.16}$$

Since $R = R(S_b)$, the value of $S_b = Y/X$ at $t = 0$ must be specified. Letting $X \to 0$ in eqns. (2.2) and (2.3) gives:

$$n_1 = - \frac{\dot{Q}_s + \dot{Q}_l}{l_0(1-\sigma)R_{w1}}, \quad t = 0 \tag{2.17}$$

$$S_b = S_w \left[1 + \dot{m}_e / \dot{R}_{w1} - n_1(1-\sigma)\right]^{-1}, \quad t = 0 \tag{2.18}$$

$R_{w1}$ is the unit water catch rate of the first spray, while $n_1 = R/R_{w1}$ is the corresponding freezing fraction. The same result is obtained from a stationary icing model letting $\vec{v}_b \to 0$. If the terms $\dot{Q}_l$ and $\dot{m}_e$ are neglected in eqns. (2.17) and (2.18), these become the basic equations used in the sea spray icing module of RIGICE. Eliminating the freezing fraction, the equation of the initial brine film salinity becomes:

$$S_b = R_w S_w \left[R_w + (\dot{Q}_s + \dot{Q}_l)/ l_0 + \dot{m}_e\right]^{-1}, \quad t = 0. \tag{2.19}$$

## 2.3 Icing for selected geometries

The theory will now be applied to some simple geometries where the droplet collection efficiency and the wind and pressure field above the boundary layer are known. A curvilinear coordinate system (s,n,z) is employed (Fig. 2.1) with the s-axis parallel to

the local wind velocity, and the z-axis normal to this direction in the tangent plane of the body (positive upwards for a tilted body). The brine film velocity components along these axes are u and w respectively.

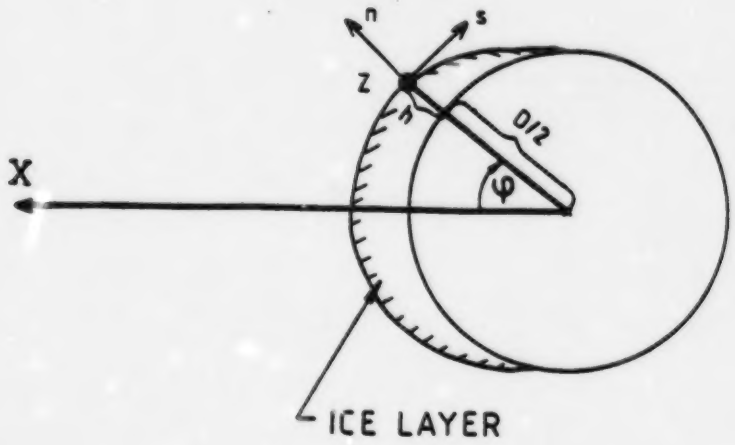


Figure 2.1: Cross section of an ice-covered cylinder showing the n,s,z axes of the curvilinear coordinate system.

2.3.1 Horizontal cylinder and plate

The geometry of this problem is shown in Figure 2.1. The brine film will only move in the s-direction and the icing equations become:

$$\frac{\partial X}{\partial t} + \frac{\partial}{\partial s}(u_b X) = R_w + \dot{m}_e - R \qquad (2.20)$$

$$\frac{\partial Y}{\partial t} + \frac{\partial}{\partial s}(u_b Y) = R_w S_w - \sigma R\, Y/X \qquad (2.21)$$

Assuming the ice grows mainly in the radial direction on cylinders

$$\frac{\partial}{\partial s} \approx \frac{2}{D_e}\frac{\partial}{\partial \varphi}$$

where $D_e$ is the "effective diameter" defined by:

$$D_e = D + \frac{2}{\pi} \int_{-\pi/2}^{\pi/2} h(\varphi)\, d\varphi \qquad (2.22)$$

From Horjen and Vefsnmo (1987) the brine film velocity may be approximated by

$$u_b = \frac{X}{\mu_b \rho_b} \left[ \frac{\tau_b}{2} - \frac{X}{3} \left( \rho_b^{-1} \frac{\partial P}{\partial s} + g \cos\varphi \right) \right] \quad \text{(cylinder)} \qquad (2.23a)$$

and

$$u_b = \frac{\tau_b X}{2\mu_b \rho_b} \quad \text{(plate)} \qquad (2.23b)$$

where $\tau_b$ is the sum of the "spray" and wind stress acting on the brine film, while P is the sum of the "spray" and wind pressure:

$$\tau_b = U_{sp} R_w + \frac{1}{2} C_f \rho_a U^2 \qquad (kg/ms^2)$$

$$P = - V_{sp} R_w - \frac{1}{2} \rho_a U^2 \qquad (kg/ms^2)$$

$U_{sp}$ and $V_{sp}$ refer to the bulk spray velocity at the moment of impact in the s- and n-direction respectively. Approximate expressions for these terms are given in Horjen and Vefsnmo (1987) assuming homogeneous droplet sizes. $C_f$ is the air/brine film friction coefficient (see Schlicting, 1955). For simplicity, the local wind velocity is calculated assuming a potential flow field:

$$U = 2 U_0 \sin \varphi \qquad (2.24)$$

2.3.2 Vertical plate

Assuming the brine film moves only downwards, the icing equations become:

$$\frac{\partial X}{\partial t} + \frac{\partial}{\partial z} (w_b X) = R_w + \dot{m}_e - R \qquad (2.25)$$

$$\frac{\partial Y}{\partial t} + \frac{\partial}{\partial z} (w_b Y) = R_w S_w - \sigma R\, Y/X \qquad (2.26)$$

The brine film velocity can now be approximated by (Horjen and Vefsnmo, 1987):

$$w_b = -0.264 \frac{g}{\rho_b \mu_b} X^2 \qquad (2.27)$$

2.3.3 Vertical cylinder

Due to the combined effect of wind/spray stress and gravity, the brine film velocity will generally have a component in both the s- and z-directions. However, this problem can be simplified somewhat by only calculating ice growth along the stagnation line. At this location, the brine film only moves downwards and the equations are the same as for a vertical plate. In order to calculate ice growth on the entire cylinder, some assumptions have to be made about the shape of the ice accretion profile. If, for example, the ice grows only on the windward side of the cylinder, and wind direction is constant throughout the icing period (T), the accumulated ice mass can be calculated from:

$$M(T) = D \int_0^T \left[ \int_{z_0(t)}^{z_m} R_0(z,t)\, dz \right] dt \qquad (2.28)$$

where $R_0$ is the stagnation line icing intensity, and $z_0$ is the lowest level of icing. This is assumed to correspond to the significant wave height

$$z_0 = H_s/2 \qquad (2.29)$$

For $z < z_0$, it is assumed that accreted ice is washed away by wave action.

Boundary conditions:

The numerical method of solution demands that boundary conditions have to be specified at both ends of the icing area. At the leading edge (s = 0) of a horizontal plate and at the top ($z = z_m$) of a vertical plate or cylinder, the boundary condition follows from the physical necessity that the brine film thickness must be zero at these places. The brine film salinity is then given by the initial value expression (eqn. 2.19). Other boundary conditions

for plates and cylinders cannot be derived from physical arguments. Instead, it is simply assumed that the second derivatives of the unknowns are zero . This can also be thought of as a "smoothing condition". The boundary conditions are therefore:

Horizontal plate:

$$X = Y = 0, \qquad s = 0$$

$$\frac{\partial^2 X}{\partial s^2} = \frac{\partial^2 Y}{\partial s^2} = 0, \quad s = L$$

Vertical plate/cylinder:

$$X = Y = 0, \qquad z = z_m$$

$$\frac{\partial^2 X}{\partial z^2} = \frac{\partial^2 Y}{\partial z^2} = 0, \quad z = z_0 \text{ (lower level)}$$

Horizontal cylinder:

$$\frac{\partial^2 X}{\partial \varphi^2} = \frac{\partial^2 Y}{\partial \varphi^2}, = 0, \quad \varphi = \pm \pi/2$$

It turns out that these assumed boundary conditions give quite reasonable results i.e. continuous changes in ice thickness in the s or z directions.

Figure 2.2. is an example of ICEMOD response for three spray cycles of a vessel deck icing simulation (assuming the brine film is at rest). The environmental conditions simulated were spray duration 6.8 seconds, salinity 34°/oo, sea-surface temperature 4°C, wind speed 25 m/s and vessel speed 7 knots. A number of features of the model are evident. First, icing and salinity are constant during the initial period of spraying (ICEMOD is equivalent to a stationary model such as RIGICE at time t=0, because the brine film thickness is zero). Icing then increases sharply after each spray due to the interruption of heat input from the warm water (spray cooling during flight is minimal for these cases). However, the brine film salinity also increases

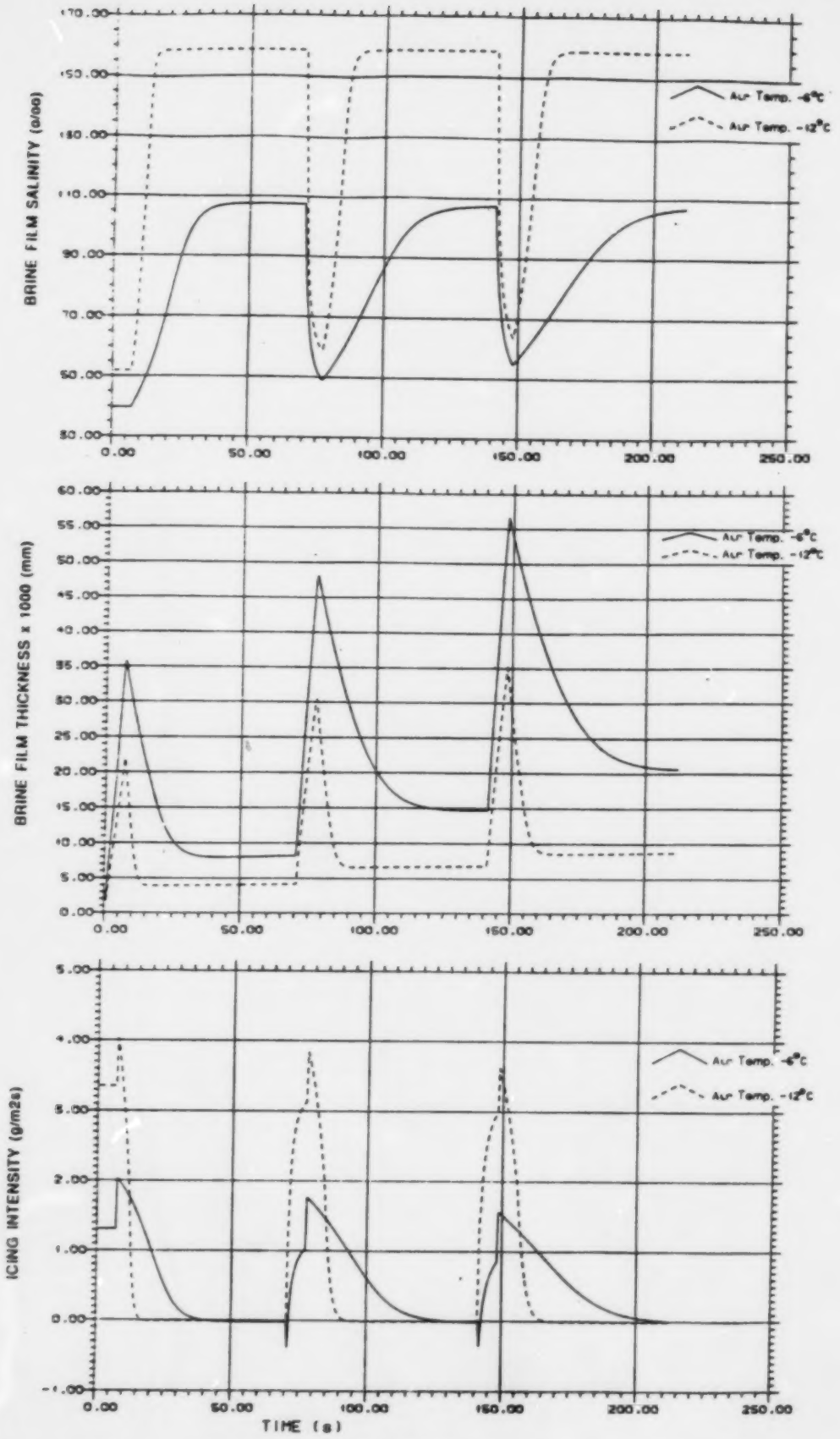


Figure 2.2: ICEMOD response for 3 spray cycles of a vessel deck icing simulation.

sharply in response to the increased accretion rate, and acts to slow down icing until it is completely cut off. The model results also show a slight melting of the accretion at the commencement of the second and subsequent sprays. The reasons for this are not clear, but it may be in response to the heat contained in a new spray.

## 2.4 Impinging spray flux

A theoretical formula for the vertical distribution of average spray mass flux generated by wave impact upon an offshore rig column is given in Horjen and Vefsnmo (1985a). The formula was fitted to empirical data from the drilling platform TREASURE SCOUT (Jørgensen et al., 1986) and has the following form:

$$G_I = f(U_{10}, H_s, z) \quad (kg/m^2 s) \tag{2.30}$$

At high wind velocities, wind-generated spray must also be considered. Based on the results of Wu et al. (1984), a modified form of a formula given in Horjen and Vefsnmo (1984b) is used:

$$G_{II} = M_2 U_{10} (s_1 \exp(H_m / 2 - z) + s_2) (U_{10}/U_{cr})^{3.4}, \quad U_{10} \geq 15 \text{ m/s} \tag{2.31}$$

where $M_2 = 9.45 \cdot 10^{-6}$ kg/m$^3$

$U_{cr} = 15$ m/s

$s_1 = (d_2^2 - d_s^2)/(d_2^2 - d_1^2)$

$s_2 = (d_s^2 - d_1^2)/(d_2^2 - d_1^2)$

$d_1$ and $d_2$ are the diameter of the smallest and the largest droplet in the spray cloud, while $d_s$ is the diameter of the largest droplet in suspension. $H_m$ is the mean wave height which from a Rayleigh distribution of wave heights is given by

$$H_m = H_s \sqrt{\pi/8} \tag{2.32}$$

The spectral distribution of droplet sizes is assumed to be proportional to $d^{-2}$ (Horjen and Vefsnmo, 1984a). Note that in Horjen and Vefsnmo (1984b), $d_s = d_1$ and the exponent 3.8 was used

instead of 3.4. According to Roebber and Mitten (1987), the latter value gives better correlations between observed and calculated spray fluxes. Values for $d_1$ and $d_2$ of 10 μm and 700 μm were assumed following Wu (1982), while $d_s$ was estimated from Wu et al. (1984) by

$$d_s = 4.73\ U_{10} + 36 \quad (\mu m) \tag{2.33}$$

## 2.5 Model configuration

ICEMOD is implemented in FORTRAN-77. Unlike RIGICE, where accretion is computed for an entire assemblage of cylinders representing a structure, ICEMOD computes accretions for single structural elements. The computed ice masses for different surfaces are combined by the user to obtain predicted ice loads on a structure such as a drilling platform. The required input parameters for running ICEMOD for rig icing simulations are (Vefsnmo, 1986):

- geometry of the icing object (cylinder/plate)
- orientation of icing object relative to wind (deg.)
- characteristic length (m)
- max. height above waterline (m)
- min. height above waterline (m)
- step length in vertical or horizontal (m)
- time step (s)
- spray horizontal flight distance (m)
- spray duration (s)
- air temperature (°C)
- sea temperature (°C)
- wind speed (m/s)
- significant wave height (m) and period (s)
- relative humidity or dewpoint temperature
- air pressure (kPa)
- spray salinity (°/oo)
- time interval between meteorological observations (hour)

The spray frequency is calculated from the assumption that every second significant wave (or more precisely, the zero upcrossing wave) produces spray. The spray frequency will then typically be in the order of 3-7 sprays/min. Data collected from the drilling platform TREASURE SCOUT seem to confirm this assumption (Jørgensen et al., 1986). If $T_s$ is the zero upcrossing wave period (s), the spray frequency is expressed by

$$N = 60 / (2\ T_s) \quad (min^{-1}) \qquad (2.34)$$

The duration of each spray is assumed to be 2 seconds based on field observations. The horizontal impact-generated spray mass flux is calculated from a formula given in Horjen and Vefsnmo (1985a) which is based on the assumption that half of the spray droplets move upwards at the moment of impact, while the other half descend. The formula is fitted to spray flux data collected at the TREASURE SCOUT (Jørgensen et al., 1986). Cooling of ascending droplets is neglected since they take a very short time to reach the top of their trajectory. On large structural elements such as drilling platform columns, the model uses a time step of 0.1 s and a length step of 0.25 m. The turbulent wind flow above the sea surface is assumed to follow a logarithmic law where the wind stress coefficient is estimated following Wu (1980).

Ice loads on the lee side of columns are computed from equation (2.28) assuming the intercepted spray flux is 10% of the upwind spray flux (Jørgensen et al., 1986), and $R_0$ is the icing intensity along the lee side stagnation line. This incorporates computation of heat transfer from the lee side of a cylinder - see Appendix A eqn. (A11).

ICEMOD produces tabular output of ice load, ice thickness and mean ice density for each elevation step. Because of the complex numerical techniques used to solve the icing intensity, ICEMOD is very CPU intensive. For example, it took about 10.3 hours of CPU time on a ND-500 mainframe computer to simulate a drilling platform icing event lasting 170 hours (the OCEAN BOUNTY "A" event described in Section 4.3). This translates to about 3.6 minutes of CPU time per hour of simulation.

## 3.0 RIGICE

In 1984, the Hydrometeorology and Marine Division of AES initiated a modest program to gain an understanding of the nature and severity of marine icing conditions in Canadian waters. This led to the publication of an assessment of the marine icing problem in Canadian waters for offshore exploration and transportation (Brown and Roebber, 1985), and the holding of an international workshop on offshore winds and icing (Agnew and Swail eds., 1985). The consensus of Canadian offshore oil operators emerging from these initial investigations was that icing was more of a nuisance than a problem for oil exploration activities off Nova Scotia and on the Grand Banks. However, government regulatory agencies such as the Canadian Oil and Gas Lands Administration (COGLA) and the Canadian Coast Guard (CCG) indicated there was a need to be able to determine icing norms and extremes for offshore structures located in Canadian waters.

Following recommendations made at the 1985 icing workshop, AES awarded a contract to The MEP Company in 1986 to develop an icing model for offshore structures. RIGICE, completed in 1987, is a stationary icing model based on the structural segmentation approach of Horjen and Vefsnmo (1984). The model incorporates Makkonen's (1985a) boundary layer model for calculating the heat transfer from the front half of a cylinder. Salinity effects and spongy ice are included in the heat balance following Makkonen (1985b). Because of budgetary constraints (the model was developed for under $25,000) and the desire to have a model which could run on a PC, the model necessarily contains many more simplifications than ICEMOD. The main differences from ICEMOD are:

(1) Icing is considered to be a continuous, steady-state process.

(2) The only structural elements considered are cylinders.

(3) RIGICE uses time-averaged spray flux expressions derived from measurements on Japanese fishing vessels, while ICEMOD uses empirical expressions obtained from data collected on drilling platforms.

(4) RIGICE assumes ice accretes uniformly over all structural members i.e. it has no special conditions for predicting 'lee' side icing as in ICEMOD.

(5) RIGICE treats inclined members the same as vertical members unlike ICEMOD where inclination is an important factor in computing brine film velocity.

(6) RIGICE assumes a constant droplet diameter of 2 mm and assumes droplet cooling is negligible. In ICEMOD, the median droplet diameter is used which is obtained from an empirical droplet size distribution. Droplet cooling is computed from the top of a droplet's orbit until it hits the structure.

(7) The value of the interfacial distribution coefficient in RIGICE is 0.26 while ICEMOD assumes a value of 0.34.

Complete documentation of the assumptions contained in RIGICE and their potential impact is given in Roebber and Mitten (1987).

NOMENCLATURE USED IN RIGICE:

$L_f$ = latent heat of fusion

$L_e$ = latent heat of vapourization

M = unit mass flux of water arriving at a surface from spray and run off

h = heat transfer coefficient

$H_s$ = significant wave height

R = recovery factor for viscous heating (0.79 cylinder)

U = free stream velocity

$U_\infty(x)$ = wind velocity outside boundary layer

$\theta(x)$ = angle around cylinder

$C_p$ = specific heat capacity of air at constant pressure

$C_i$ = heat capacity of ice

$C_w$ = heat capacity of water

$T_s$ = surface temperature of accreted ice

$T_a$ = air temperature

$T_d$ = dewpoint temperature

$T_w$ = temperature of impinging droplets = sea temp. in RIGICE

$\varepsilon$ = $R_v/R_d$ = ratio of molecular weights of water vapour and dry air = 0.622

$P$ = static air pressure

$e_{so}$ = saturation vapour pressure over ice surface at $T_s$

$e_a$ = saturation vapour pressure over surface at $T_d$

$S_b$ = brine salinity

$S_w$ = water salinity

$S_i$ = ice salinity

$E$ = collection efficiency

$w$ = liquid water content

$n$ = freezing fraction of impinging water

$S$ = shape factor ($2/\pi$ for cylinder)

$D$ = cylinder diameter

$a$ = radiation linearization constant ($8.1 \cdot 10^7$)

$k_a$ = thermal conductivity of air

$\rho_a$ = air density

$\rho_i$ = ice accretion density

$\sigma$ = Stefan-Boltzman constant ($5.67 \cdot 10^{-8}$ $Wm^{-2}K^{-4}$)

$\nu$ = kinematic viscosity of air

$\tau_0$ = shear stress at the wall ($y = 0$)

$\chi$ = sponginess factor = $1 - S_i/S_b$ (0.74 for $n < 1.0$)

$z$ = height above mean sea level

## 3.1 Theoretical background

The physics used in the spray icing module of RIGICE can be divided into three basic processes: (1) determine the impinging spray flux, (2) calculate the heat transfer rate, and (3) solve the heat balance to obtain the icing intensity.

3.1.1 Impinging spray flux:

As the only field data collected on spray fluxes impinging on drilling platforms (Jørgensen et al., 1986) are proprietary, it was necessary to scour the literature for suitable expression to use in RIGICE. Impact-generated spray is the most important source of spray impinging on an offshore structure (Zakrzewski, 1986). Unfortunately, all of the available expressions in the literature were derived from ships which have quite different splashing characteristics than a static arrangement of vertical columns. Roebber and Mitten (1987) evaluated a number of expressions in RIGICE and found that the following expression (Horjen and Vefsnmo, 1984), derived from Japanese trawler data (Tabata, 1969), produced the most realistic total ice loads on drilling platforms:

$$w = 0.1\ H_s \exp(H_s - 2z) \quad (kgm^{-3}) \tag{3.1}$$

Wind-generated spray is known to be a minor spray source in offshore icing (Zakrzewski, 1986). However, under certain severe conditions such as those experienced in Lower Cook Inlet by the OCEAN BOUNTY (Nauman, 1984), wind-generated spray may be important. The following expression was used from Horjen and Vefsnmo (1984):

$$w = 9.45 \cdot 10^{-6} (U_{10}/15)^{3.8} \exp(H_s/2 - z) \quad (kgm^{-3}) \tag{3.2}$$

RIGICE therefore contains the same liquid water content expressions used in the first stationary version of ICEMOD.

3.1.2 Heat Transfer:

Heat transfer from an icing cylinder is calculated following Makkonen (1985a). The theory includes the effects of increased surface roughness as icing progresses. An infinitely long cylinder of diameter D is assumed to have a steady two-dimensional incompressible boundary layer on the forward face:

$$u\frac{\partial u}{\partial x} \quad v\frac{\partial u}{\partial y} = -\frac{1}{\rho_a}\frac{\partial P}{\partial x} + \frac{1}{\rho_a}\frac{\partial \tau_0}{\partial y} \tag{3.3}$$

where u and v are the flow velocity components. The velocity distribution outside the boundary layer is assumed to be:

$$U_\infty(x) = 1.58 \sin (1.233\ \theta(x))\ U \tag{3.4}$$

where $\theta(x) = 2x/D$. Note that ICEMOD uses the potential flow approximation shown in eqn. (2.24). Integrating the boundary layer equation, and taking into account the equation of continuity and the Bernouilli equation, it can be shown that:

$$Nu_l = \frac{0.29\ D\ U_\infty^{1.435}(x)}{\nu^{0.5}\left[\int_0^x U_\infty^{1.87}(x)dx\right]^{0.5}} \tag{3.5}$$

where $Nu_l$ is the local cylinder Nusselt number for laminar flow.

By using Prandtl's mixing length theory, it is possible to obtain an expression for the shear stress $\tau_0$ at the wall surface in turbulent flow. The Stanton number for fully rough flow, St(x), is derived by substituting $\tau_0$ into the integrated momentum equation to determine the momentum thickness for the turbulent boundary layer. The local Nusselt number for the turbulent region, $Nu_t$, is then:

$$Nu_t(x) = \frac{St(x)U_\infty(x)\rho_a C_p D}{k_a} \tag{3.6}$$

The transition point between laminar and turbulent flow is determined by computing the momentum boundary layer thickness and laminar Nusselt number in 5 degree steps from 0 to 90°. The local Reynolds number is then used to test for transition to turbulent flow. The overall Nusselt number for the front half of the cylinder, $Nu_a$, is determined from the mean of all the local values of Nu:

$$Nu_m = \left[Nu(0°) + Nu_{l,m}(90°) + 2\sum_{i=1}^{17} Nu_{l,t}(51°)\right]/36 \qquad (3.7)$$

The overall heat transfer coefficient for the front half of the cylinder is then:

$$h = \frac{k_a}{D} Nu_m \qquad (3.8)$$

3.1.3 Heat Balance:

The heat balance of the icing surface is described (after Makkonen, 1984) by:

$$Q_f + Q_v + Q_h + Q_c + Q_e + Q_w + Q_s = 0 \qquad (3.9)$$

where $Q_f$ = latent heat released during freezing

$Q_v$ = frictional heating of air

$Q_h$ = artificial heating of surface to prevent icing

$Q_c$ = loss of sensible heat to air

$Q_e$ = heat loss from evaporation

$Q_w$ = heat transfer between impinging spray and the accretion surface

$Q_s$ = heat loss from radiation

The heating due to the kinetic energy of the impinging water droplets and the heat loss due to conduction are sufficiently small that they are ignored in RIGICE. Additionally, because of the large droplet sizes associated with impact-generated spray, it is assumed that droplets have the same temperature as the sea-surface and that run-down water remains at its original impact temperature.

Spongy ice is taken into account following Makkonen (1985b) by inclusion of an ice sponginess factor, $\chi$, defined as $1 - S_l/S_b$. $\chi$ is equal to 0.74 for spongy ice with shedding of unfrozen water, and ranges between 0.74 and 1.00 for spongy ice with no shedding (all impinging water freezes or is trapped in the ice). In ICEMOD, the corresponding value of $\chi$ is 0.66 since $S_l/S_b$ is taken to be

0.34. The individual terms in the heat balance used in RIGICE are:

$$Q_f = 2/\pi \; M \; n \; L_f \; \chi \tag{3.10}$$

$$Q_v = h \; R \; U^2 / \; (2 \; C_p) \tag{3.11}$$

$$Q_c = h \; (T_s - T_a) \tag{3.12}$$

$$Q_e = \frac{h\epsilon}{PC_p} \left[ e_{so}(1-0.537 \; S_b) - e_a \right] L_e \tag{3.13}$$

$$Q_w = 2/\pi \; M \; C_w \; (T_s - T_w) \tag{3.14}$$

$$Q_s = \sigma \; a \; (T_s - T_a) \tag{3.15}$$

Brine salinity is expressed as a function of temperature, x, by the following empirical function (Makkonen, pers. comm.):

$$S_b = -x/54.0 \tag{3.16}$$

The freezing fraction, n, is expressed as a function of $S_b$ and $S_w$ following Makkonen (1985b):

$$n = (S_b - S_w)/(\chi \; S_b) \tag{3.17}$$

In practice, n is obtained in RIGICE by iterating surface temperature to solve the heat balance in eqn. (3.9) with the freezing fraction eliminated. Once the equilibrium surface temperature, $T_s$, is known, n is computed from equations (3.16) and (3.17). The procedure used is (Roebber and Mitten, 1987):

1) Assume $n < 1.0$ and $\chi = 0.74$
2) Solve energy balance for $T_s$ using the bisection method
3) Compute n from equations (3.16) and (3.17)
4) Test value of n:
   a) if $n \leq 0$ then no icing
   b) if $0 < n < 1$ then $\chi = 0.74$ and there is ice accretion with runoff
   c) if $n \geq 1$ then spongy ice without runoff: set $n = 1.0$ and solve $\chi$ by iteration.

Macklin's (1962) ice density parameter is used to compute accretion density in the model. This is very likely not applicable to ice accreted offshore from saline spray, and should be changed. In practice, however, the large assumed droplet size of 2 mm results in a constant accretion density of 920 $kgm^{-3}$ which is representative of wet growth, saline accretions. Ice is initially assumed to accrete radially on vertical and diagonal columns. A weighting scheme based on wind direction variation over an icing event is then used to 'redistribute' the ice. Wind components are used for computing ice accretion amounts on the sides of the deck. Ice thickness on the underside of a drilling platform is estimated by taking the ice thickness at the top of a vertical column, scaled by $\sigma_3/U$, the ratio of the vertical wind speed turbulence to horizontal wind speed. This was given by Smith (1980) as:

$$\sigma_3/U = 0.038 + 0.001\ U, \quad \dim U = m/s \tag{3.19}$$

The model physics do not contain any ice shedding mechanisms such as structural vibration or wave impact. However, it is assumed that any ice accreted below the current value of the significant wave height is removed. This effect is only noticeable in the case of a rapidly building sea, since the liquid water content near wave crests is too high to allow freezing.

## 3.2 Model Configuration

RIGICE was designed to run interactively on an IBM AT or similar PC. Hourly meteorological and oceanographic data and drilling platform specifications are supplied to the system through a user-friendly input interface. The model has separate modules for handling sea spray icing and atmospheric icing as atmospheric icing is assumed to only accrete on the deck and superstructure, while spray icing is confined to the columns and undersides. RIGICE is thus unable to consider mixed accretion e.g. snow and freezing spray. It should be noted that in RIGICE, diagonal trusses are treated the same as vertical members except that the length increment for computing ice loads is 0.707 m instead of 0.5 m (i.e. the angle is fixed at 45°). In ICEMOD however, the inclination angle of a member is considered when computing brine

film velocity. Complete documentation of the assumptions contained in RIGICE and their potential impact is given in Roebber and Mitten (1987).

The model requires the following hourly input data:

- air temperature (°C)
- dew point temperature (°C)
- sea-surface temperature (°C)
- air pressure (mb)
- wind speed (knots) at known reference height (m)
- wind direction
- significant wave height
- significant wave period (not required for currently used liquid water content expressions)
- precipitation type (code)
- precipitation intensity (code)
- sea water salinity (°/oo)

The precipitation type and intensity codes are described in Roebber and Mitten (1987) and are used to assign precipitation intensities and droplet sizes.

For a full drilling platform structural specification, RIGICE performs two hours of simulation per minute on an IBM AT with a math co-processor. Because of memory size limitations, the maximum length of event which can be handled is 186 hours. After a simulation is completed, the following products are available to the user:

- plots of ice thickness profiles on vertical and diagonal columns;
- a time series plot of total ice load on the structure;
- a table of total ice loads and maximum ice thicknesses on individual structural elements.

In addition, time series plots are available of the meteorological and oceanographic data for each icing event.

## 4.0 MODEL EVALUATION

The evaluation of the two models was carried out at three levels. First, a sensitivity analysis was performed to assess the internal consistency of model response for typical icing conditions.

Second, model response was investigated under the controlled environment of a wind tunnel. And lastly, the models were run for a number of drilling platform icing case studies with hourly meteorological and oceanographic data.

## 4.1 Sensitivity analysis

Due to the non-linearity of the icing process, two standard conditions were utilized to investigate model response: one typical of North Sea icing conditions, and a second more typical of icing conditions experienced off the east coast of Canada and in the Barents Sea. These are summarized in Table 4.1 ("East Coast" standard condition in parentheses).

Table 4.1

Standard conditions used in the sensitivity analyses.

| Standard condition | Range | Step |
|---|---|---|
| $T_a$ = -4.0°C (-10.0) | 0 to -20.0°C | 2°C |
| $T_w$ = 4.0°C (0.0) | -2.0 to 6.0°C | 1°C |
| $U_{10}$ = 20.0 m/s | 5 to 35 m/s | 5 m/s |
| $S_w$ = 34.8 °/oo | 0 to 40 °/oo | 5 °/oo |
| RH = 90% (80) | 10 to 90% | 10% |
| D = 10.0 m | 1.5 to 10.0 m | 1.5, 5.0, 10.0 m |
| $\theta$ = 90° | 45 to 90° | 45, 90° |

$\theta$ = cylinder orientation w.r.t. horizontal

The model output selected for comparison was total ice load on a 10.0 m diameter vertical cylinder of 20.0 m length, for an icing duration of one hour. Air pressure was kept constant at 100.0 kPa in all runs. RIGICE was run using a time-averaged liquid water content with a single 60 minute time step. A shorter time step was not required in RIGICE because the only time-dependent effect included in the model is the feedback from increasing conductor diameter which is only significant for cylinder diameters of several cm or less. A 0.1 s time step was used in ICEMOD and gravity was assumed to be the only external force acting on the brine film i.e. wind and spray stress effects on the brine film

were ignored.

One problem encountered in the sensitivity analysis was that ICEMOD uses proprietary empirical expressions to obtain spray flux information as a function of wave height, wind speed, wave period, elevation and time. RIGICE, on the other hand, uses a simple time-averaged liquid water content expression based on wave height and elevation. To run both models with some common liquid water content expression would have created "artificial" results which were not representative of the way the models perform in actual icing simulations. Therefore, to minimize differences in model input data as much as possible, yet retain the characteristics of each model, the sensitivity analyses were performed using a common method for prescribing significant wave height and period i.e. the 3rd-degree polynomial expressions presented in Zakrzewski (1986) for a 200 nautical mile fetch. The equation used for significant wave height was

$$H_s = 4.22 \cdot 10^{-1} - 7.75 \cdot 10^{-2} U_{10} + 3.47 \cdot 10^{-2} U_{10}^2 - 5.72 \cdot 10^{-4} U_{10}^3 \qquad (4.1)$$

The sensitivity results for increasing wind speed thus incorporate the effect of increasing wave height in both models. The results of the sensitivity analysis are presented in Figures 4.1 to 4.4 for the "North Sea" standard condition, and in Figures 4.5 to 4.8 for the "East Coast" standard condition. The salient features and significant differences between the two models are discussed below:

4.1.1 North Sea Condition:

The model responses are quite similar for the warmer sea-surface and air temperatures employed in this standard condition. The most notable differences occur for sea-surface temperature (Fig. 4.2) and wind speed (Fig. 4.3). RIGICE displayed much greater sensitivity to sea-surface temperature than ICEMOD, particularly for temperatures less than 0°C. This difference is considered to be due to the heat transfer between the impinging spray and the surface brine film, $\dot{Q}_w$: in RIGICE, this term is active during the entire icing period while in ICEMOD, $\dot{Q}_w$ is zero between sprays. In

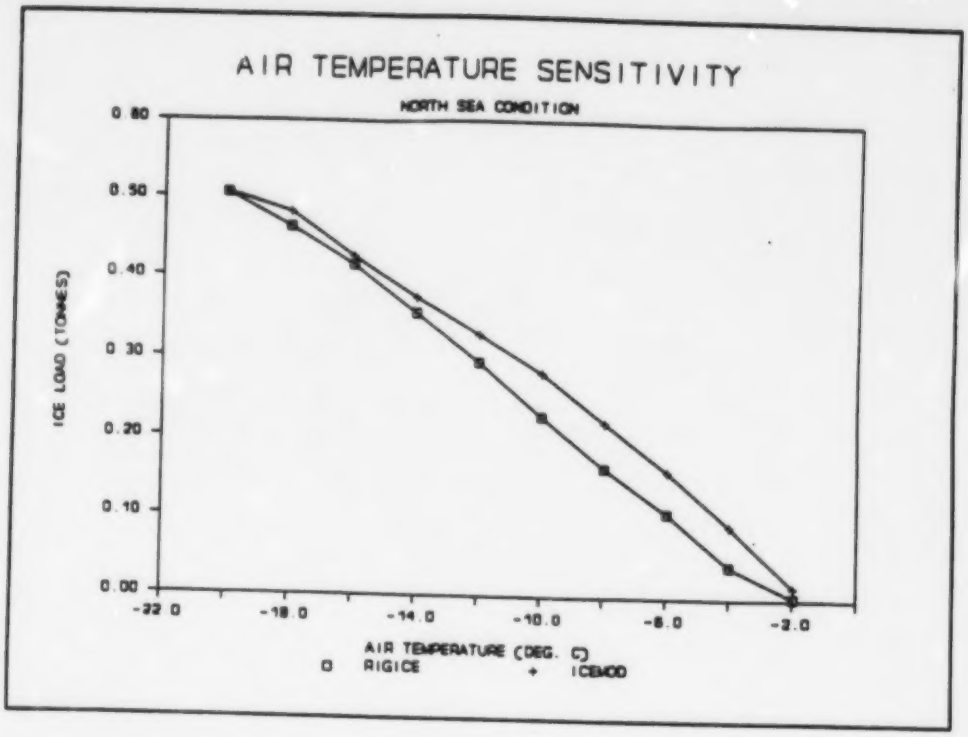


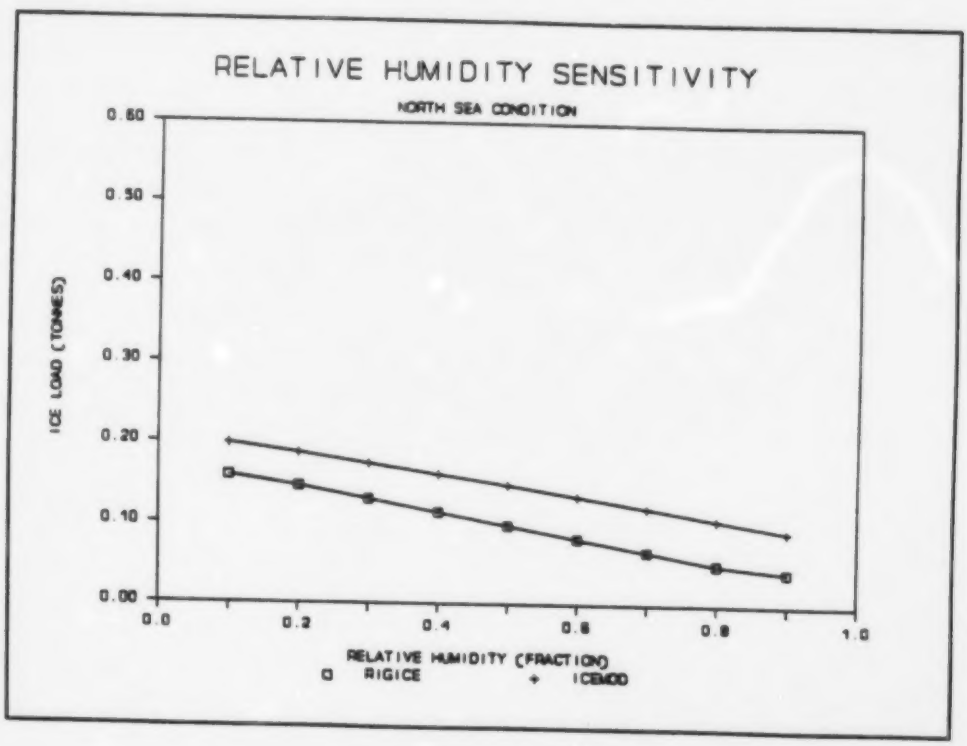


**Figure 4.1:** RIGICE and ICEMOD sensitivity to changing air temperature and relative humidity for the North Sea test condition.

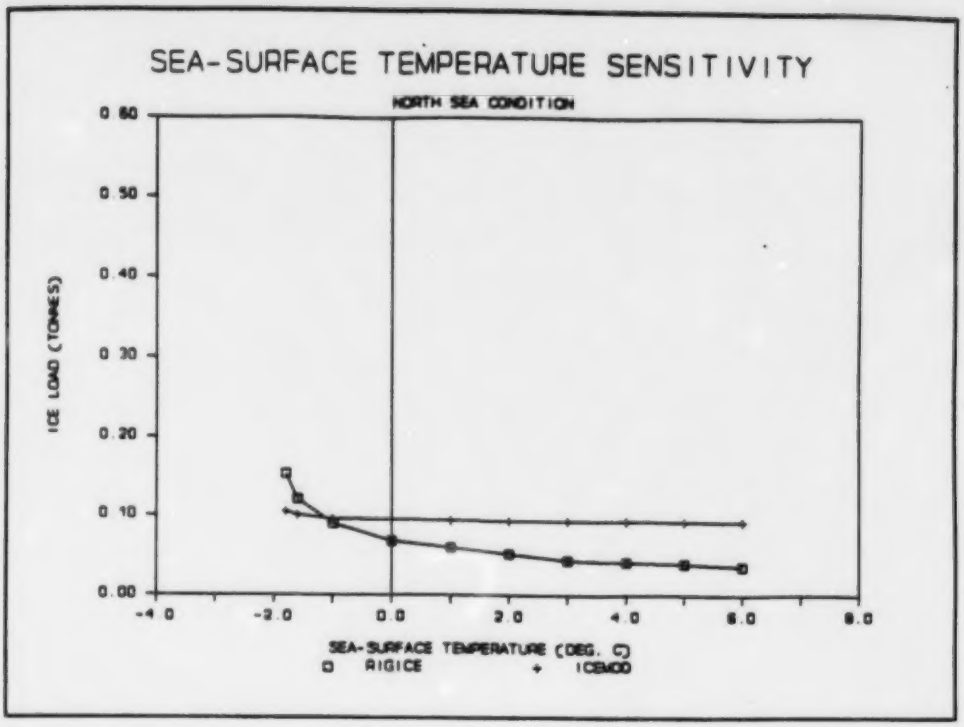


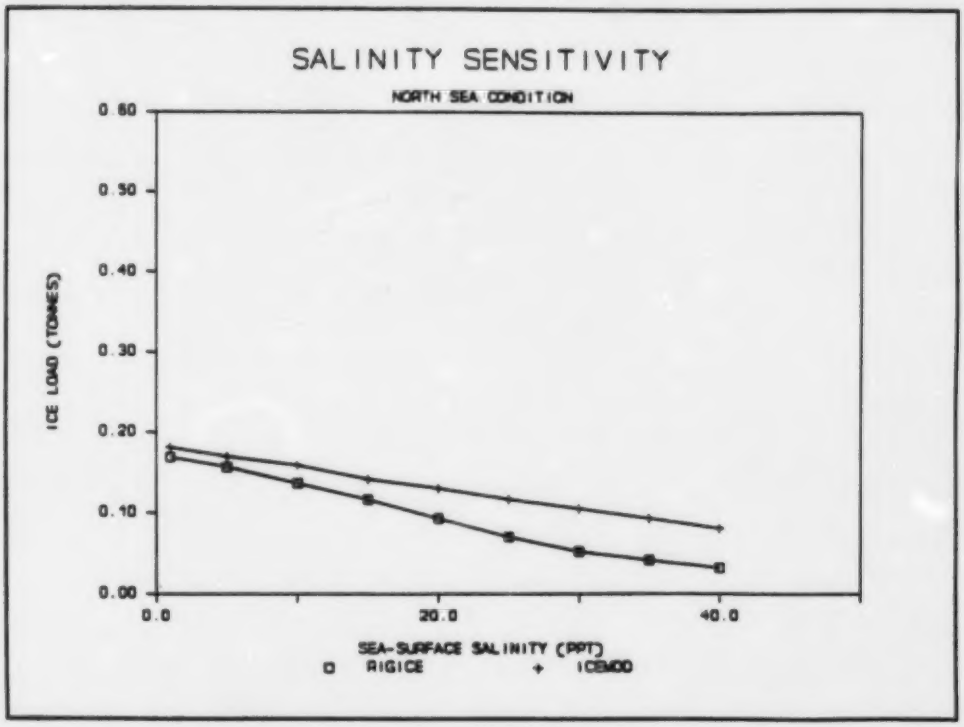


**Figure 4.2:** RIGICE and ICEMOD sensitivity to changing sea-surface temperature and salinity for the North Sea test condition.

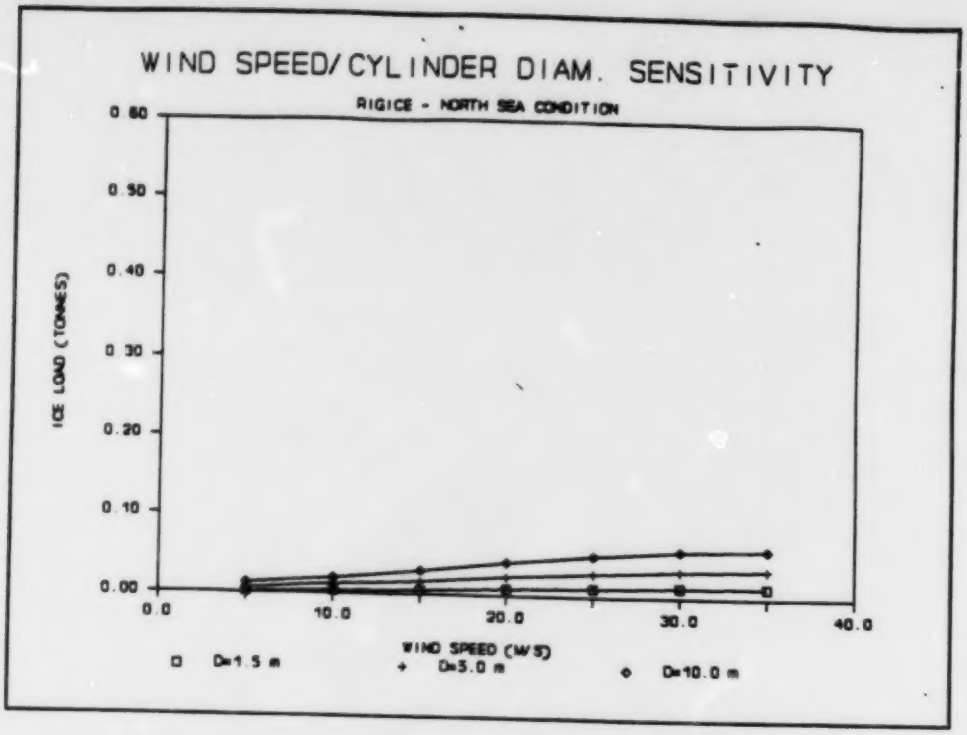


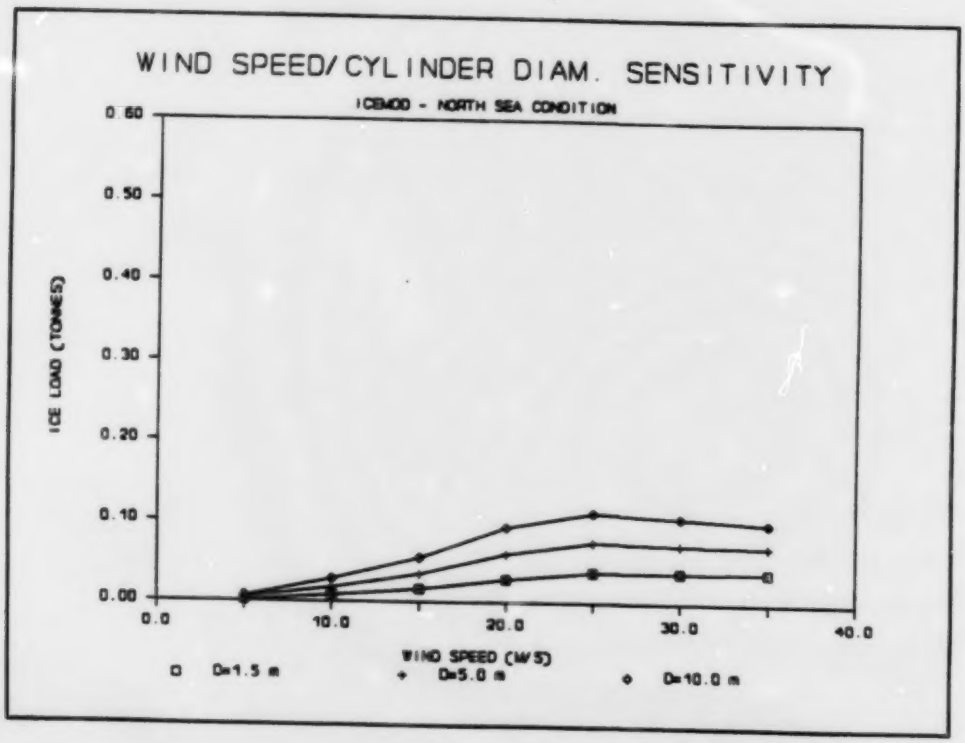


**Figure 4.3:** RIGICE and ICEMOD sensitivity to changing wind speed and cylinder diameter for the North Sea test condition.

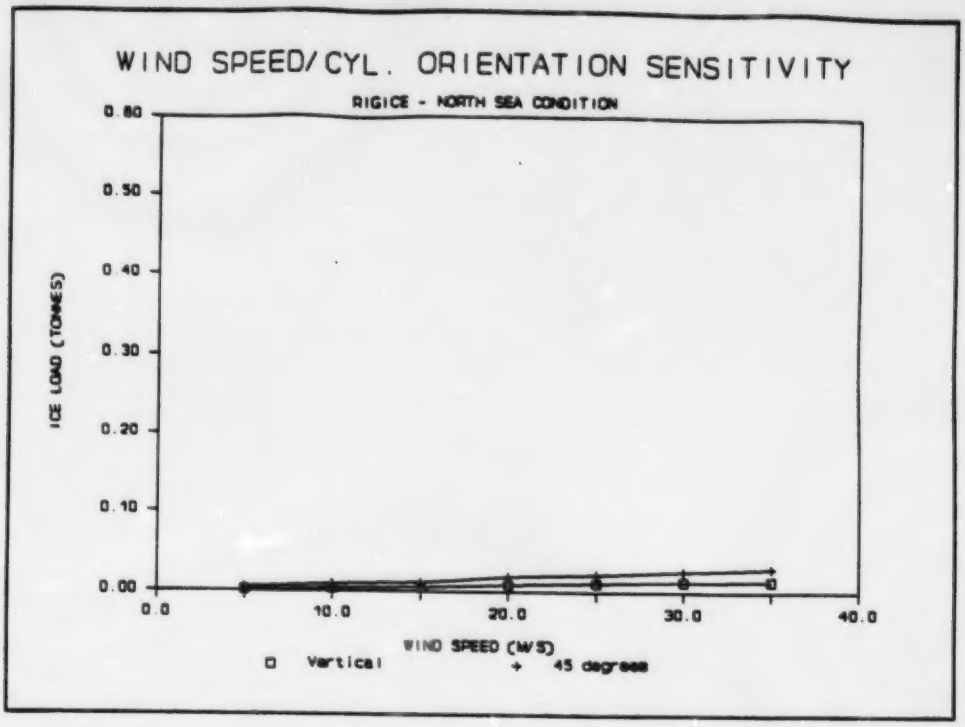


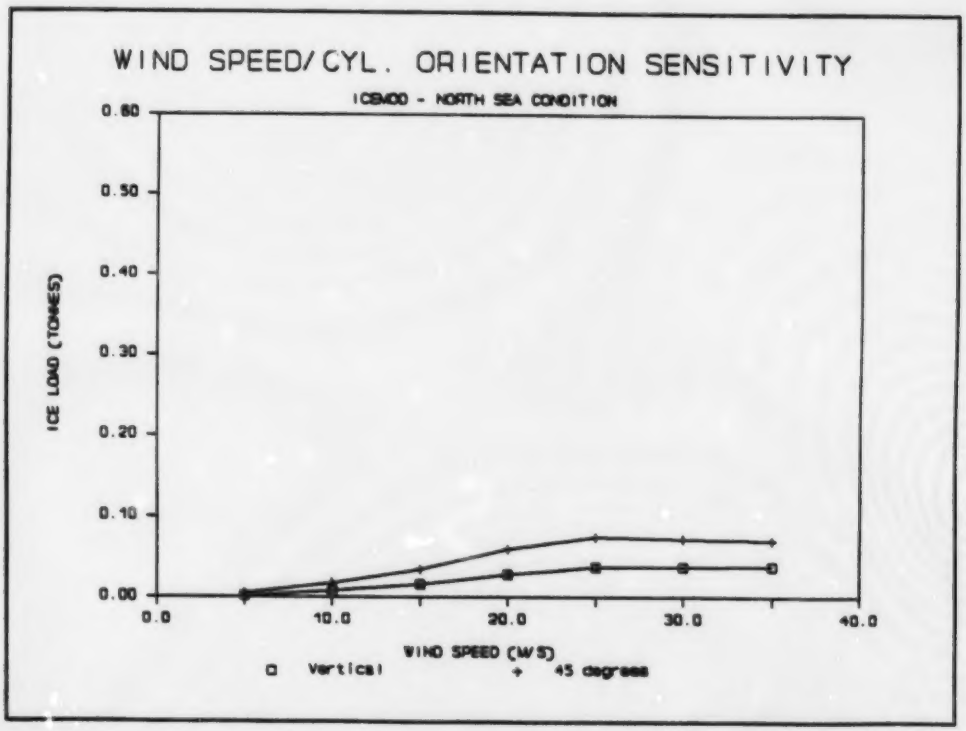


**Figure 4.4:** RIGICE and ICEMOD sensitivity to changing cylinder orientation for the North Sea test condition (D=1.5 m).

addition, ICEMOD includes the time-dependent feedback mechanism of increasing brine film salinity after each spray which acts to regulate the icing rate. ICEMOD displayed greater sensitivity to increasing wind speed (and liquid water content) than RIGICE, and actually showed a decrease in ice loads for the 5.0 and 10.0 m diameter cylinders when wind speed exceeded 25 m/s. The decrease is the result of the heat contained in the increased liquid water flux arriving at the cylinder becoming more significant than corresponding heat loss terms.

4.1.2 East Coast Condition:

The colder air and sea-surface temperatures of the East Coast standard condition showed up significant differences in model response for changing salinity, sea-surface temperature and air temperature. The different model responses to changing sea-surface temperature (Fig. 4.6) are a clear demonstration of the impact of the time-dependent effects included in ICEMOD. Without these, RIGICE displayed an exponential growth in accreted ice loads as sea surface temperature decreased below a value of ~ 0°C. This feature was also observed in the Stallabrass (1980) model which assumes icing is a stationary process. The sensitivity of stationary models to colder sea-surface temperatures may also explain some of the discrepancies noted by Roebber and Mitten (1987) when evaluating model performance for icing data sets collected from areas with different sea temperature regimes e.g. the Gulf of Alaska and the east coast of Canada.

Fig. 4.6 shows RIGICE also had an exponential response to decreasing sea-surface salinity below values of ~ 20 °/oo for the colder east coast conditions, in marked contrast to the North Sea response (it should be noted that the physics in RIGICE becomes unstable for salinities less than about 0.1 °/oo). It was difficult to determine the exact cause for this response due to the large number of interdependent processes operating in the model. The Stallabrass (1980) model applied to a vertical cylinder (ignoring rundown salinity) exhibited a similar exponential increase in ice load as salinity approached that of fresh water. The heightened salinity sensitivity of stationary models compared

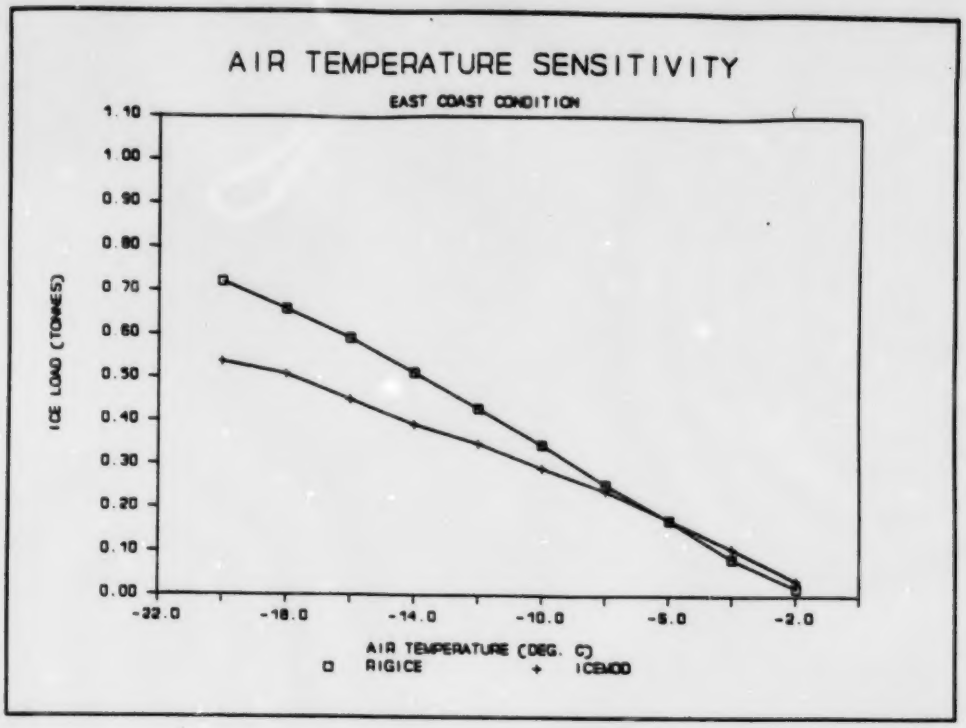


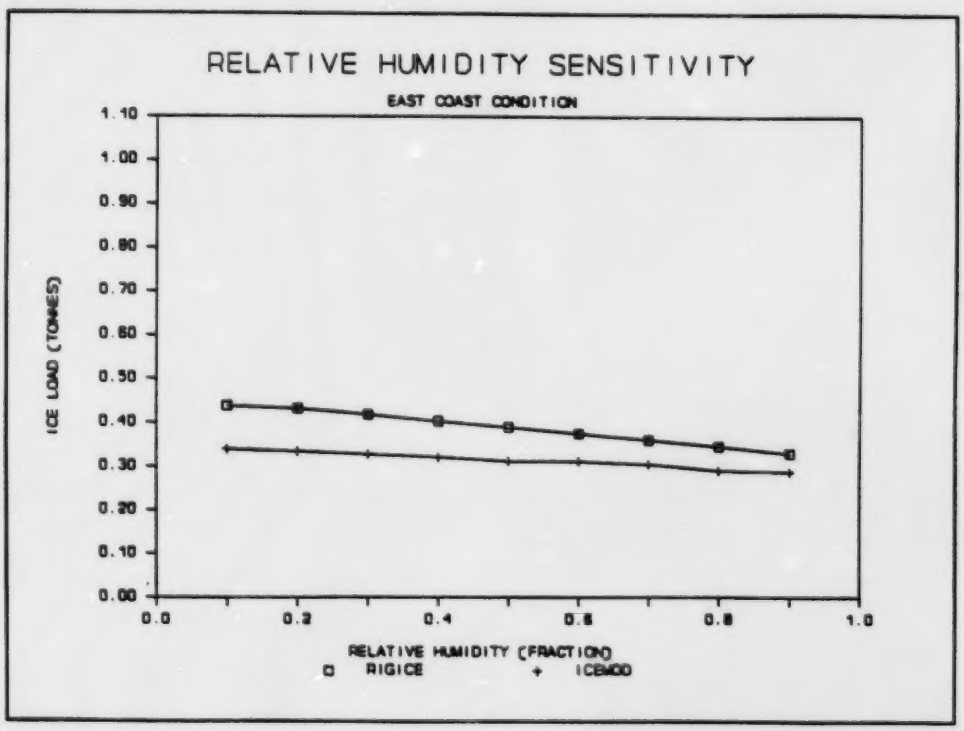


**Figure 4.5:** RIGICE and ICEMOD sensitivity to changing air temperature and relative humidity for the East Coast test condition.

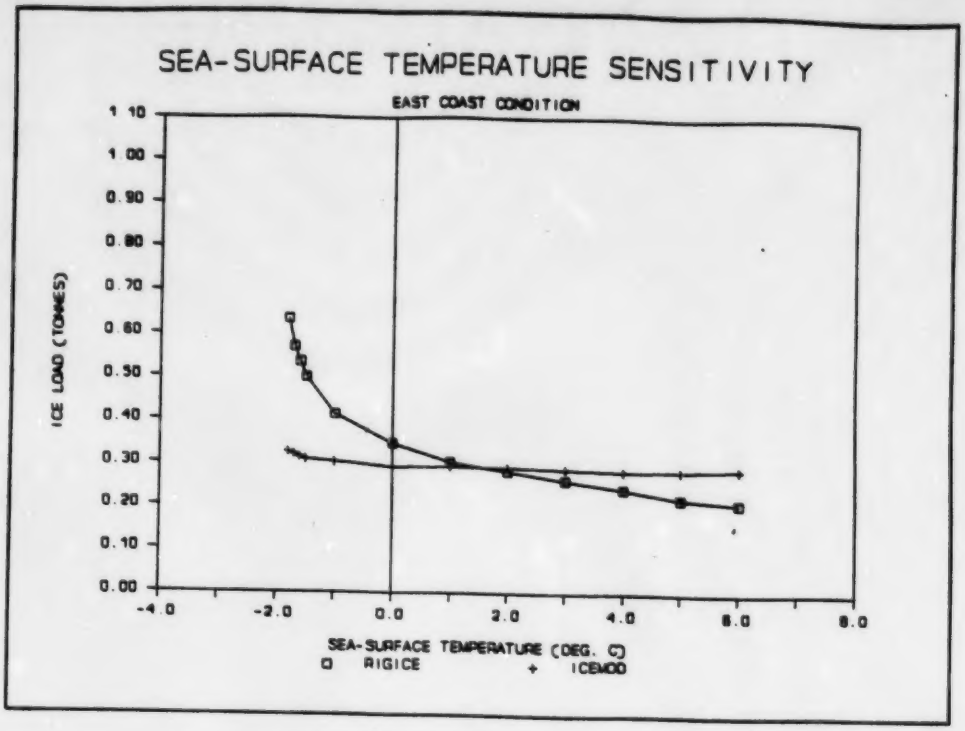


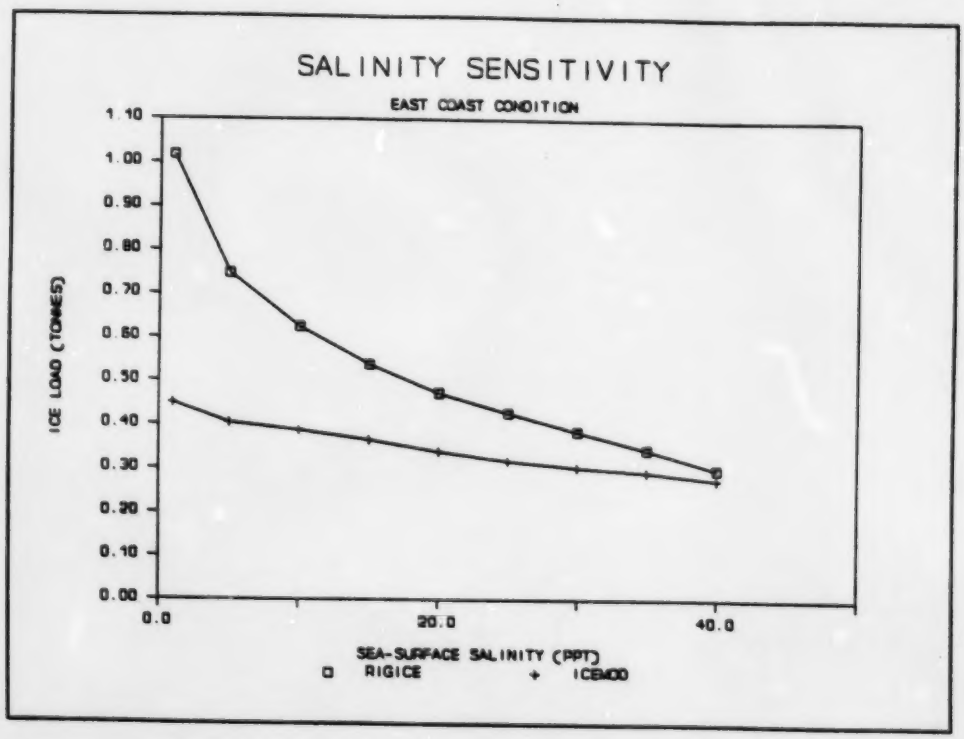


**Figure 4.6:** RIGICE and ICEMOD sensitivity to changing sea-surface temperature and salinity for the East Coast test condition.

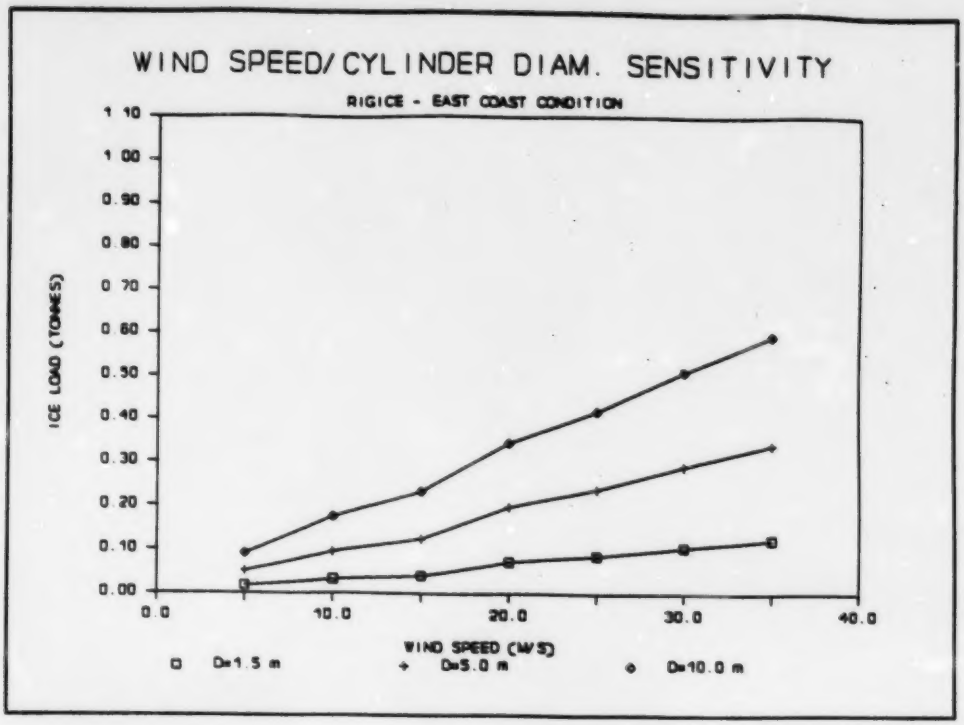


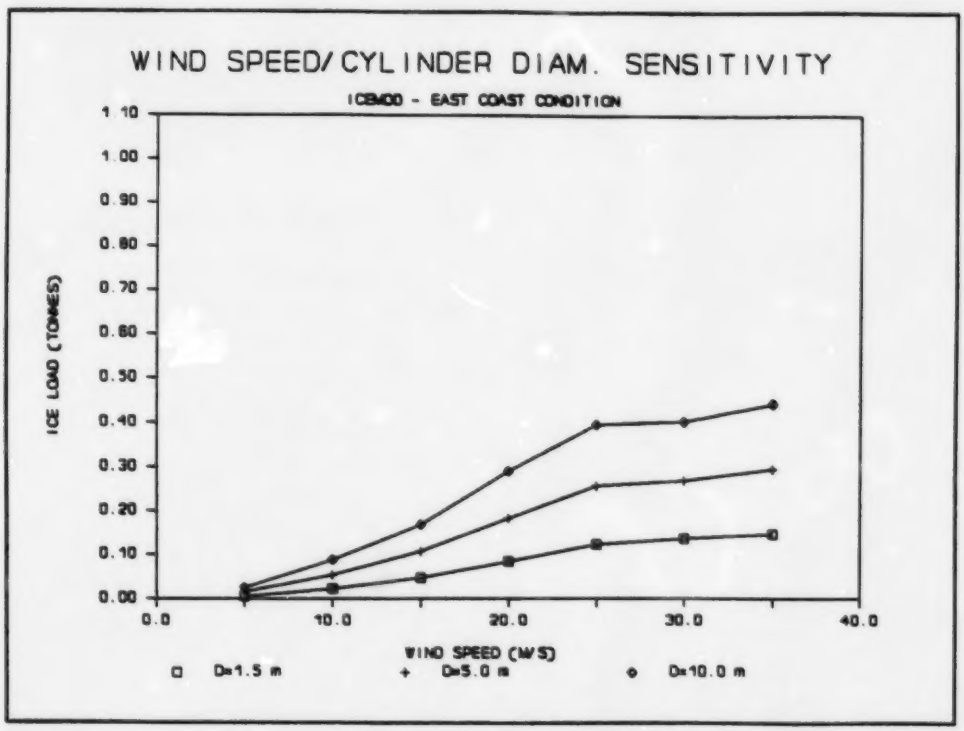


**Figure 4.7:** RIGICE and ICEMOD sensitivity to changing wind speed and cylinder diameter for the East Coast test condition.

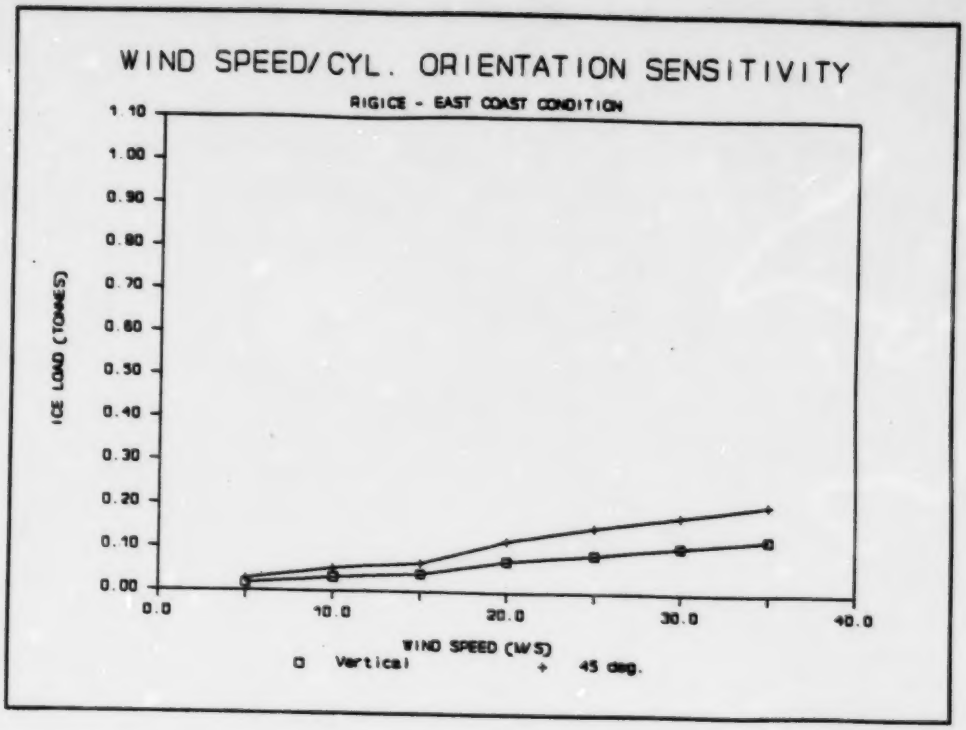


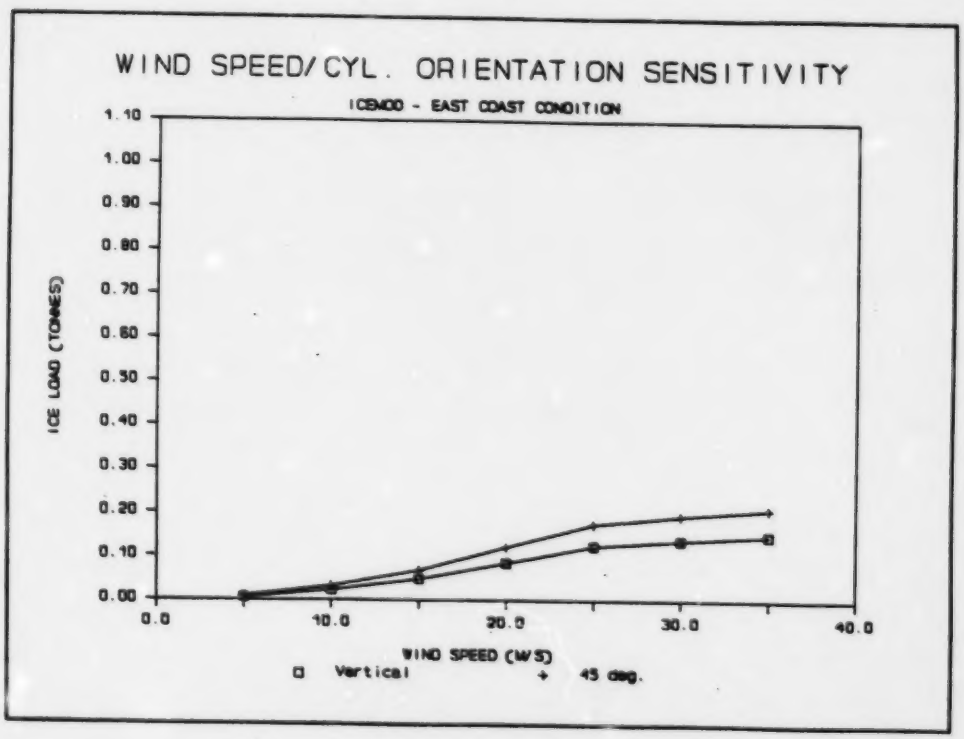


**Figure 4.8**: RIGICE and ICEMOD sensitivity to changing cylinder orientation for the East Coast test condition (D=1.5 m).

to ICEMOD raises some questions about the universal applicability of stationary spray icing models in cold water environments.

The above sensitivity results suggest that RIGICE and ICEMOD are likely to predict similar ice loads where sea-surface temperatures are above 0°C, and sea-surface salinities are in the 30-40 °/oo range typical for oceanic waters. However, for colder sea-surface temperatures and low salinities, it is clear that the equilibrium surface temperature approach used to solve the surface heat and salt balances in RIGICE (and other stationary icing models) is likely to overpredict ice loads.

## 4.2 Wind tunnel simulations

An outdoor wind tunnel facility was constructed at NHL during 1984 with the express purpose of conducting icing experiments with saline water. The facility is described in Carstens et al. (1984) and has the following characteristics:

| | |
|---|---|
| Total length: | 25.0 m |
| Length test section: | 9.0 m |
| Diameter test section | 1.4 m |
| Test cross section | 1.5 $m^2$ |
| Max. air velocity | 30.0 m/s |

Air temperature and relative humidity in the tunnel were the same as ambient conditions. Spray was produced from a spray rig positioned in the inlet contraction with salt water fed from a temperature controlled tank. A pre-programmed magnetic valve controlled spray frequency and duration, while liquid water content and droplet size were varied using different spray nozzles.

### 4.2.1 Experimental conditions

During the winter of 1985/86, NHL carried out several pulsed spray experiments in the wind tunnel to calibrate ICEMOD. The test object was a 50 mm diameter non-rotating horizontal cylinder placed in the centre of the tunnel. All experiments were carried out with a Spray System GA3 nozzle which produces spray clouds with a median volume droplet diameter of 1.0 mm. In all tests, spray frequency was 3 sprays per minute, with a spray duration of

2 seconds per spray. These values were selected based on field observations of spray characteristics on offshore drilling platforms.

The water catch rate in the tunnel was measured with absorption panels for three different wind velocities. Mean results from three sets of measurements are shown in Table 4.2. The relationship between the measured time-averaged water flux on a plate, $\bar{R}_w^{pl}$, and the average water flux on the upwind side of a cylinder in one spray is given by Horjen and Vefsnmo (1986b) as:

$$\bar{R}_w^{cyl} = \frac{2\, E_c^{cyl}\, \bar{R}_w^{pl}}{\pi\, E_c^{pl}\, N\, t_s} \qquad (4.2)$$

where $E_c^{cyl}$ = collection efficiency of cylinder
$E_c^{pl}$ = collection efficiency of plate
$N$ = spray frequency
$t_s$ = duration of one spray

RIGICE requires the average liquid water content of the free air stream ($\overline{LWC}$) as input. Assuming $E_c^{pl} \approx 1$, this is obtained from $\bar{R}_w^{pl} / U$.

Table 4.2

Water flux measurements in the icing tunnel

| U (m/s) | $\bar{R}_w^{pl}$ (g/m$^2$s) | $\overline{LWC}$ (kg/m$^3$) |
|---|---|---|
| 10 | 2.00 ± 0.24 | $2.000 \cdot 10^{-4}$ |
| 20 | 3.39 ± 0.06 | $1.695 \cdot 10^{-4}$ |
| 25 | 4.55 ± 0.14 | $1.820 \cdot 10^{-4}$ |

The following parameters were kept constant during the experiments:

Cylinder diameter : 50 mm
Cylinder length : 17 cm
Droplet diameter : 1 mm

| | |
|---|---|
| Spray frequency | : 3 sprays/minute |
| Spray duration | : 2 seconds |
| Water temperature | : 4°C |
| Icing duration | : 60 minutes |

Wind velocity, spray salinity, air temperature and relative humidity were varied in the experiments. However, only the U = 25 m/s experimental results with sea water (salinity ~ 34 °/oo) were available for the latest version of ICEMOD for comparison with RIGICE. A relatively short icing duration was used because air temperature and relative humidity are unable to be controlled in the outdoor wind tunnel.

For the wind tunnel experiments, ICEMOD employed a 0.005 s time step, a 10° angle step, and wind and spray stress effects were included in the computation of brine film movement around the cylinder. Two different configurations of RIGICE were used in the pulsed spray experiments: (1) the "average liquid water content" mode used in the sensitivity analysis where icing is assumed to take place over the entire period (this uses the $\overline{LWC}$ values in Table 4.2), and (2) a "peak liquid water content" mode where icing only takes place during each spray (this uses 10 times the average liquid water content for an icing duration of 360 seconds). A 60 s time step was used in the peak LWC configuration of RIGICE, while the average LWC configuration used a single 1 hour time step.

### 4.2.2 Results

RIGICE and ICEMOD results for the pulsed spray experiments are presented in Figure 4.9. It is clear that neither of the two RIGICE model configurations were as successful as ICEMOD in predicting ice loads under pulsed spray conditions. The results demonstrate the need to address both in-spray and between-spray icing processes: according to Horjen and Vefsnmo (1987), the main difference between a stationary (peak LWC) and time dependent model is the freezing of the water film between two sprays. It is also apparent that the average LWC version of RIGICE greatly overpredicts ice loads over a wide range of conditions. This particular model configuration only gives reasonable results when icing is in the dry growth mode. However, the peak LWC

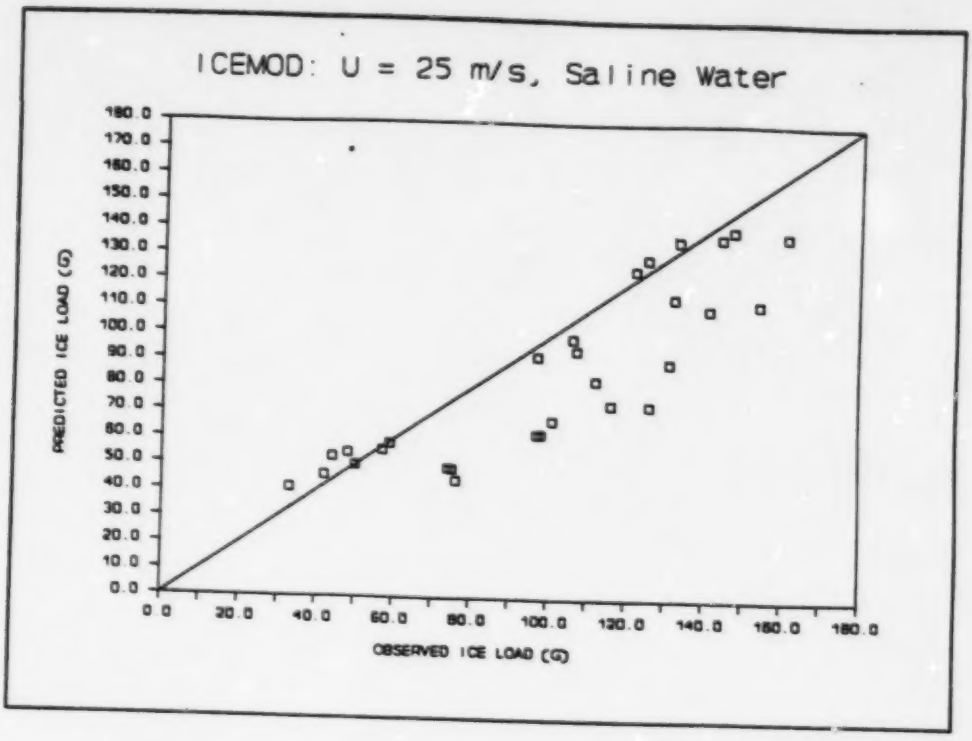


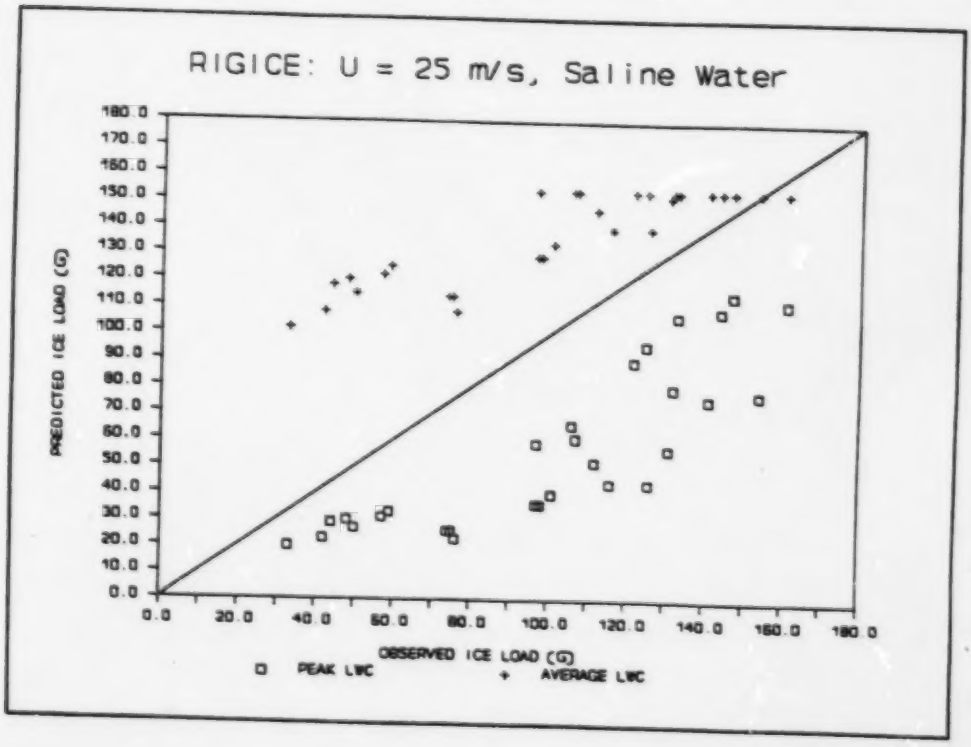


**Figure 4.9:** ICEMOD and RIGICE ice load results for the saline, pulsed spray wind tunnel experiments.

configuration underestimates ice loads even where conditions are conducive to dry growth.

While the peak LWC configuration of RIGICE underpredicted ice loads, it exhibited a surprisingly similar model response to ICEMOD. The inter-model $r^2$ value was 0.987 and a plot of the two model results (Fig. 4.10) yielded a clear curvilinear relationship. This suggested that it may be possible to "calibrate" stationary models as a function of the freezing fraction. Replotting model results expressed in terms of freezing fractions (Fig. 4.11) produced the following least squares relationship

$$n_{td} = 1.13\ n_{st}^{0.71}, \quad n_{st} \leq 0.84 \quad (r^2 = 0.996) \qquad (4.3)$$

where $n_{td}$ is the time-dependent model event freezing fraction, and $n_{st}$ is the stationary model event freezing fraction. While eqn. (4.3) looks promising, it is unlikely to be applicable to offshore icing events. First, the wind tunnel experiments were carried out for a set of fixed conditions e.g. fixed spray frequency, spray duration and droplet size, which will not be replicated offshore. Second, the experiments were performed with a horizontal cylinder which may reduce the impact of time-dependent effects resulting from vertical brine film movement.

## 4.3 Drilling platform icing cases

The successful performance of a model in the controlled environment of a wind tunnel is one thing. However, the real test of a model is how well it works in the field with routinely collected meteorological and oceanographic data as input. There are a number of documented drilling platform icing events in the literature e.g. Nauman (1984) and Minsk (1984). However, little effort has been expended to try and evaluate icing models for such cases mainly because of poor documentation of ice thicknesses and loads on offshore drilling platforms. This situation is a reflection of the physical difficulties associated with trying to obtain icing measurements on the underside of a rig, and the absence of any successful, inexpensive measuring device able to

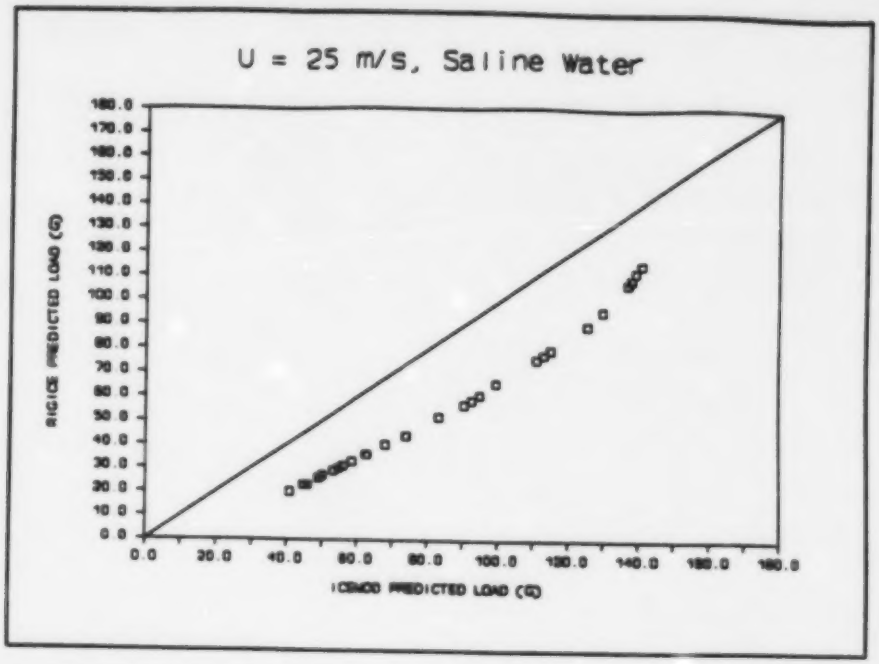


**Figure 4.10:** Comparison of RIGICE (peak LWC) and ICEMOD results for one set of pulsed spray icing experiments on a horizontal cylinder.

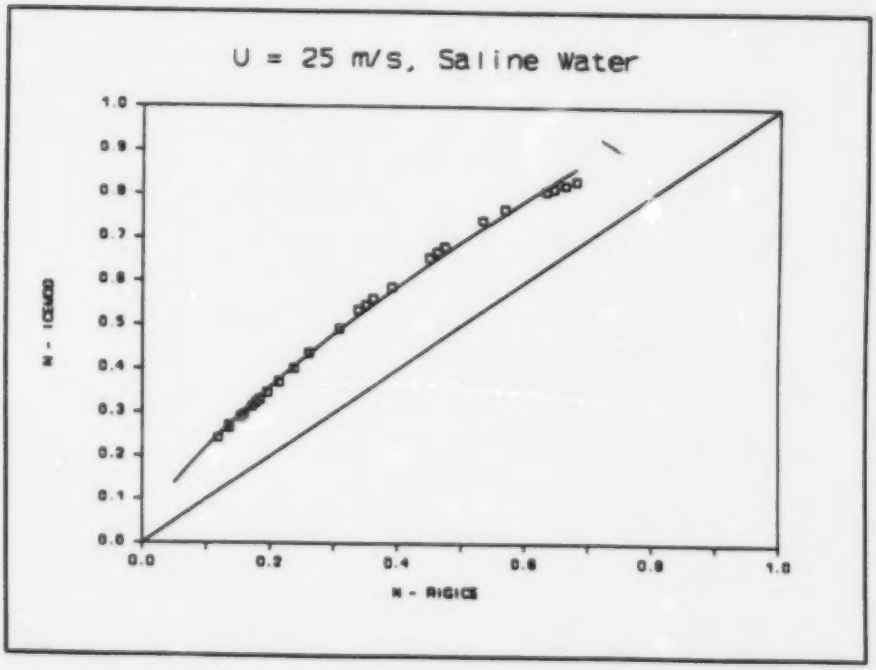


**Figure 4.11:** The same results expressed as freezing fractions with the best fit expression of equation (4.3).

withstand the rigors of deployment in the wave wash zone.

AES established a drilling platform icing monitoring program in the winter of 1985/86 to try and obtain better icing information for model evaluation purposes. Due to budget restrictions, the program relied on photography and ice thickness estimates obtained by rig-based weather observers and supply vessel personnel. These data are not ideally suited for model evaluation purposes (estimated total ice loads in particular) because of varying degrees of subjectivity. However, they are the best available, and can be used to obtain a reasonable idea of the performance of a particular model. Of the available documented platform icing events, 7 were selected which had some of the best quality ice accretion data. These events are summarized in Table 4.3 while individual event descriptions are presented below:

SEDCO 708, January 4-6, 1983.

This event occurred while the semi-submersible SEDCO 708 was operating in the Gulf of Alaska at 56.3°N, 161.8°W. David Minsk of CRREL was on board at the time to document platform icing: a description of the event is given in Minsk (1984). A data logger system was in operation on the SEDCO 708 to record environmental data at a 20 minute interval. Unfortunately, the logger air temperature data became erratic at 1200 LST (Local Standard Time) on January 6, just as the main period of icing began. Additional air temperature data were available in the form of aviation weather reports (Form 10) taken hourly from 0400 to 1700 LST. A default sea-surface salinity of 32.5 °/₀₀ was taken from the Soviet World Ocean Atlas.

This event was difficult to document because of some confusion between LST and GMT (Greenwich Mean Time) e.g. in Figure 6 in Minsk (1984), the present weather reports should all be shifted 11 hours to the left to match the logger data which are recorded on LST. While conditions conducive to icing persisted until January 8, the photos used to document the event were taken between 1310 and 1450 LST on January 6. Model input data are therefore terminated at 1500 LST on this day. Ice thickness profiles on a

Table 4.3

Summary of drilling platform icing events.

| Platform | Location | Period* (hours) | Max. U (m/s) | Max. $H_s$ (m) | Min. $T_a$ (°C) | Avg. $T_s$ (°C) |
|---|---|---|---|---|---|---|
| SEDCO 708 | Bering Sea | 60 | 20.7 | 5.4 | -8.3 | 3.7 |
| SEDCO 709 | Scotian Shelf | 48 | 19.0 | 2.1 | -10.0 | 1.7 |
| SEDCO 710 | Grand Banks | 63 | 23.1 | 7.0 | -16.0 | -0.8 |
| BOW DRILL 1 | Grand Banks | 72 | 24.2 | 6.5 | -13.0 | 0.5 |
| BOW DRILL 3 | Grand Banks | 71 | 29.8 | 7.0 | -12.3 | -0.2 |
| ROWAN GORILLA | Scotian Shelf | 9 | 25.2 | 4.4 | -6.7 | 6.0 |
| OCEAN BOUNTY | Cook Inlet | 169 | 50.4 | 4.9 | -16.1 | 5.5 |

* Duration of icing conditions used in model comparisons

windward column and diagonal truss were estimated from the photos given in Minsk (1984). Minsk estimated a total ice accretion load of 27 tonnes from photographs. Time series plots of the main environmental parameters affecting the icing process up to 1500 LST on January 6 are shown in Figure 4.12. The ice accretion data for this event allowed model comparisons of vertical ice thickness profiles on windward columns and diagonal trusses, and comparisons of the total ice load estimate provided by Minsk for 1500 LST on January 6.

SEDCO 709 "B", January 24-26, 1986.

This event was documented by the drilling platform ice and weather observer (MacLaren Plansearch, 1986) while the SEDCO 709 was drilling on the Scotian Shelf at 43.7°N, 59.9°W. Hourly meteorological and oceanographic data for the event were compiled from hourly environmental logs maintained by the observer. All data were measured on an hourly basis except sea-surface temperatures which were measured every 3 hours. A typical salinity of 34 °/oo was assumed for the event. Plots of the main parameters controlling ice accretion are presented in Figure 4.13. Icing on diagonal trusses, wooden bumpers and anchor chains was first noted by the observer at 1500 GMT on January 24. Icing was initially confined to the windward side of the rig, but by 0600 GMT on January 25, icing was noted to have started on the downwind columns. Maximum ice build-ups were reported at 1800 GMT on the 25th with 15-20 cm estimated on diagonal trusses and 7-10 cm on anchor chains and wooden bumpers. Ice was noted to extend 7.0 meters above the waterline. A number of photographs were taken of the main columns and diagonal trusses at 1800Z on the 25th. Unfortunately, there were insufficient photos to derive a mass estimate. However, some useful information was obtained from the photographs namely, the vertical distribution and thickness of ice on a windward column, and the maximum thickness of ice on a diagonal truss. The observer provided an estimate of 31.0 tonnes for the total mass of accreted ice. The observer reported no further ice accretion at 0300Z on the 26th, and that accreted ice was falling off in large sheets three hours later at 0600 GMT. Although there are no measured icing data for this event, it has

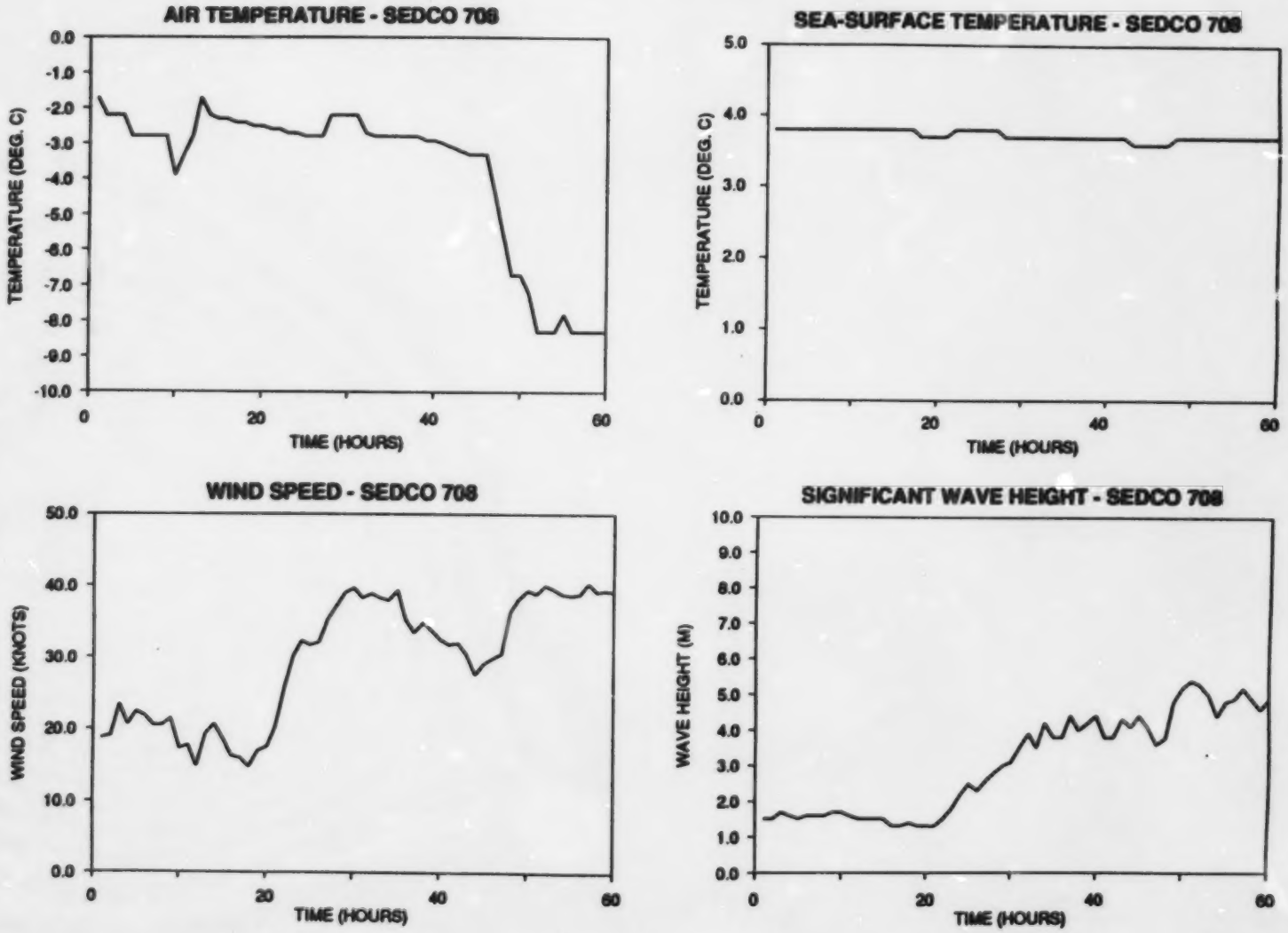


**Figure 4.12:** Meteorological and oceanographic conditions during the SEDCO 708 icing event.

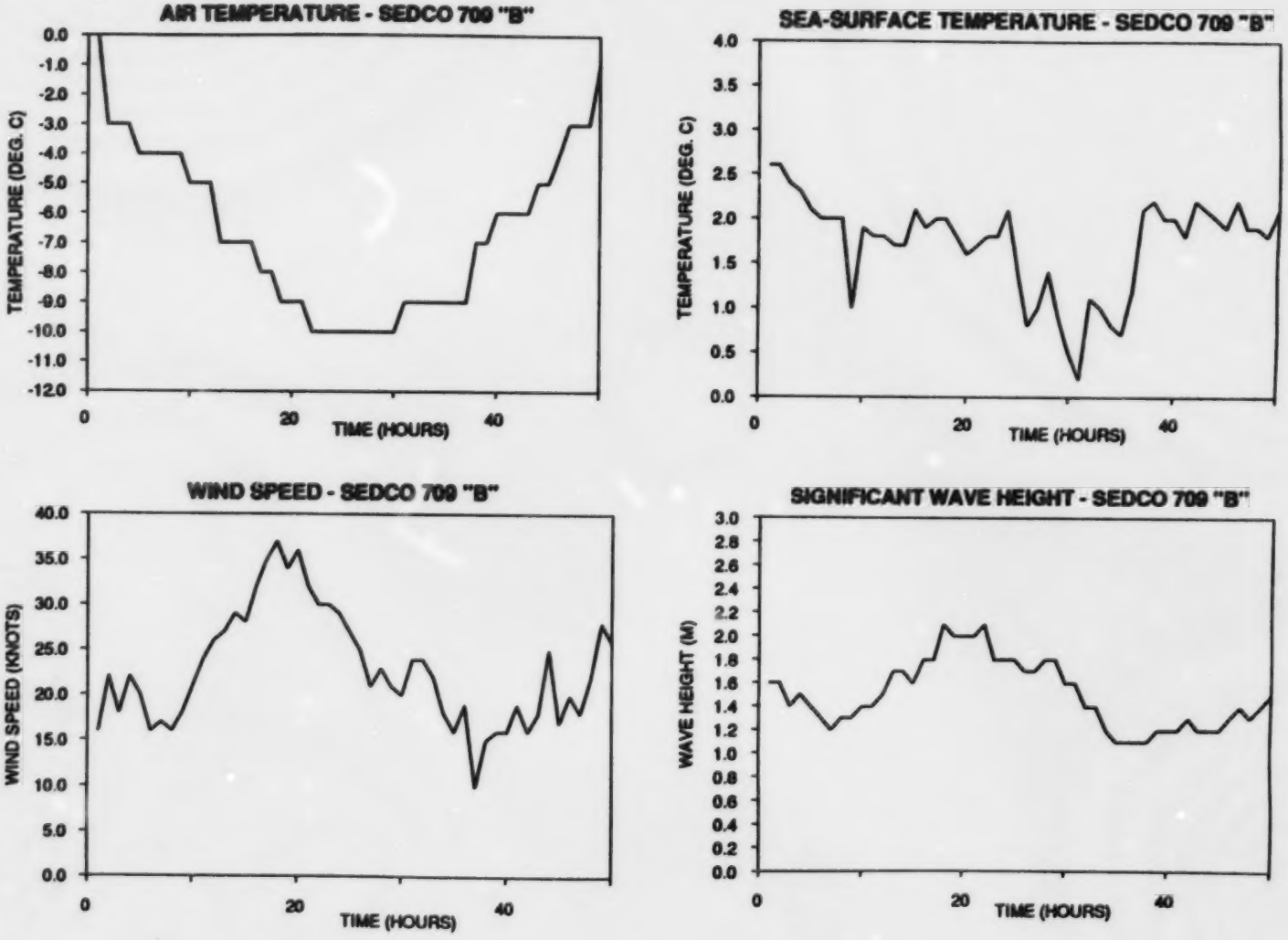


**Figure 4.13:** Meteorological and oceanographic conditions during the SEDCO 709 "B" icing event.

the most detailed icing chronology of all the rig icing events obtained for model evaluation. In addition, the model input data are probably the best available from a a routine observing program. For this event, the models were run up to 1800 GMT on January 25 and ice thickness profiles compared for the windward columns. The models were then run for the entire icing period and the total ice loads compared with the observer's estimate.

SEDCO 710 "B", March 8-12, 1986.

This event was selected because it had the highest reported ice load (52 tonnes) from two years of available Canadian Coast Guard Mobile Offshore Drilling Unit (MODU) icing report forms. The event took place over a period of several days while the SEDCO 710 was drilling on the Grand Banks (46.6°N, 48.4°W). Hourly model input data were interpolated from 3-hourly marine weather reports. A typical salinity of 34 °/oo was assumed for this event. However, it was subsequently determined that a number of recorded sea-surface temperatures (-1.9°C values) were lower than was theoretically possible for the assumed salinity level, which caused RIGICE to greatly over-estimate the ice accretion rate. These values were therefore read as -1.8°C by RIGICE to maintain consistency with the assumed salinity. Time series plots of the main environmental parameters affecting the icing process are shown in Figure 4.14.

The ice and weather observer indicated icing began at 2300 GMT on March 9, and ended at 2330 GMT March 11. No photographs are available for this event. However, the observer indicated ice extended up to 9.0 mASL, and that there was an average of 5.0-7.5 cm ice on ladders and anchor chains, and 7.5-10.0 cm on columns. An ice load estimate of 52.0 tonnes was given by the observer based on an ice thickness/ice load look-up table prepared for the rig by the operator. The models were run for the entire icing event to compare predicted ice loads and thicknesses with the observer's estimates.

BOW DRILL 1, December 26-29, 1984.

This event took place while the drilling platform BOW DRILL 1 was

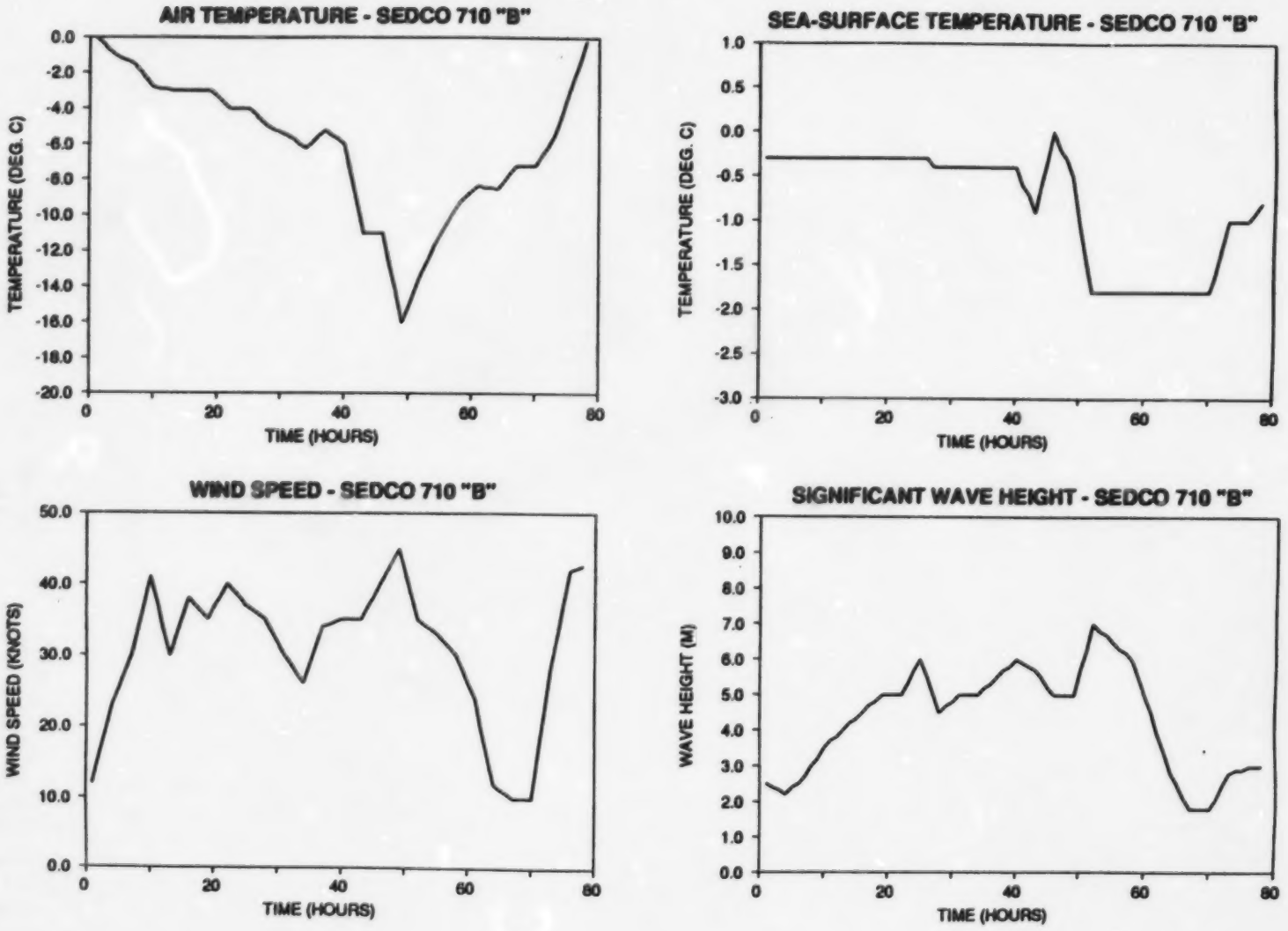


**Figure 4.14:** Meteorological and oceanographic conditions during the SEDCO 710 icing event.

operating at the West Ben Nevis B-75 wellsite on the Grand Banks at 46.5°N, 48.4°W. Good quality 3-hourly environmental data were available which were interpolated to hourly data for the model simulations (Fig. 4.15). A typical sea-surface salinity of 34 °/oo was assumed for the model runs. This event was not particularly well documented in terms of ice accretion data. However, the event is of some interest because it affected two drilling platforms (BOW DRILL 1 and BOW DRILL 3) located less than 25 km apart. The observer indicated this event resulted in light freezing spray with 2.5-5.0 cm of ice on main columns, with ice extending up to 7.0 m above sea level. An ice load estimate of 10 tonnes was provided based on an ice thickness/ice load look-up table prepared for the rig by the operator. The models were run with the entire period of data for this event, and the total loads compared with the observer's estimate.

BOW DRILL 3, December 26-29, 1984.

This event was selected because the BOW DRILL 3 was located close to the BOW DRILL 1 (~25 km) during the same icing event, yet appeared to have accreted considerably more ice. This was considered to be a good test case for the models.

The event took place while the drilling platform BOW DRILL 3 was operating at the North Ben Nevis P-93 wellsite on the Grand Banks at 46.7°N, 48.4°W. Good quality 3-hourly environmental data were available which were interpolated to hourly data for the model simulations (Fig. 4.16). A typical sea-surface salinity of 34 °/oo was assumed for the model runs. The observer indicated the event resulted in light freezing spray with 5.0-7.5 cm of ice on main columns, and >10.0 cm on diagonal trusses. Ice was indicated to extend up to 12.0 m above sea level. An ice load estimate of 20 tonnes was provided based on an ice thickness/ice load look-up table prepared for the rig by the operator. The models were run with the entire period of data for this event, and the total loads compared with the observer's estimate.

ROWAN GORILLA I, December 19-20, 1985.

This event occurred while the jack-up drilling platform ROWAN

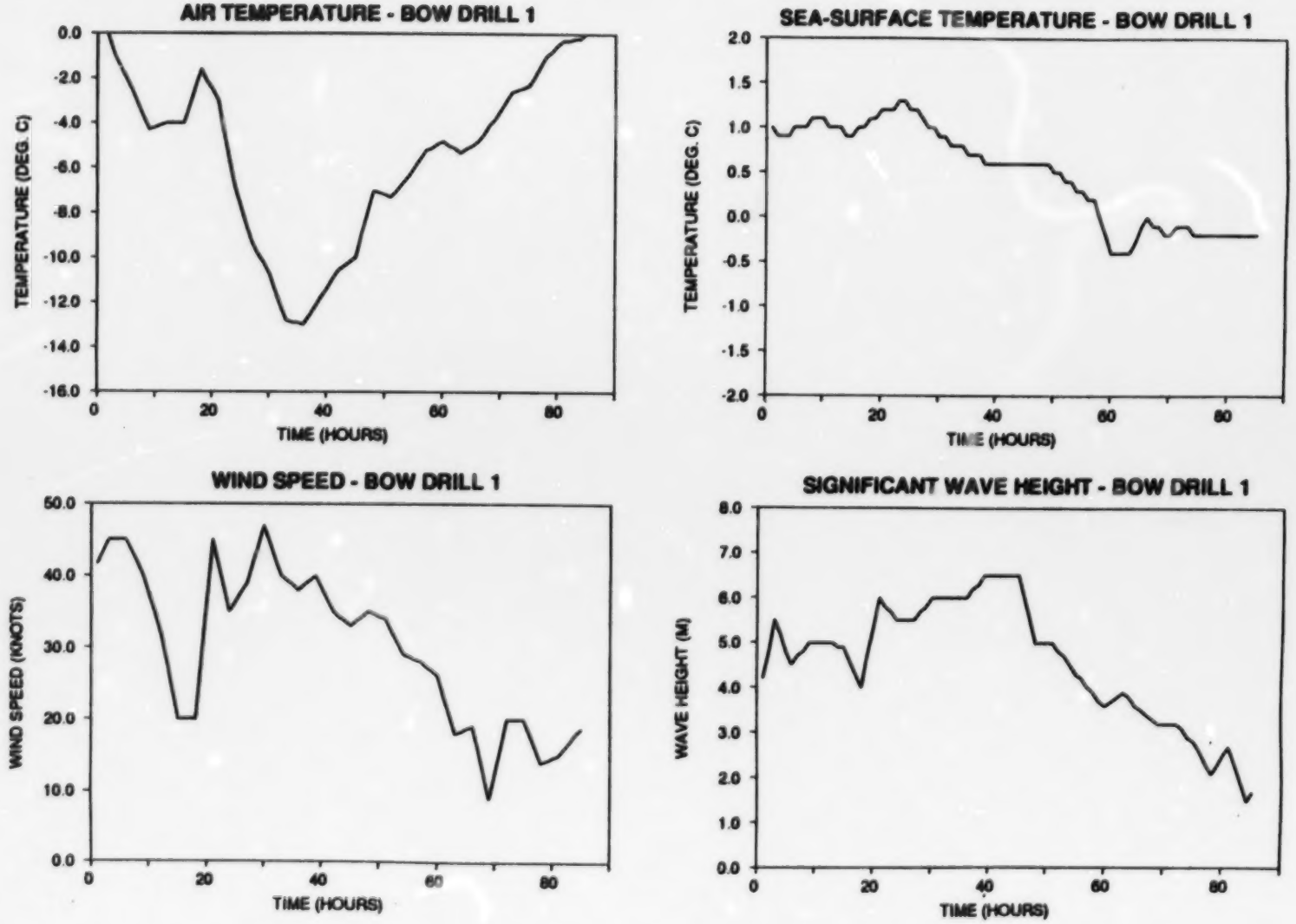


**Figure 4.15:** Meteorological and oceanographic conditions during the BOW DRILL 1 icing event.

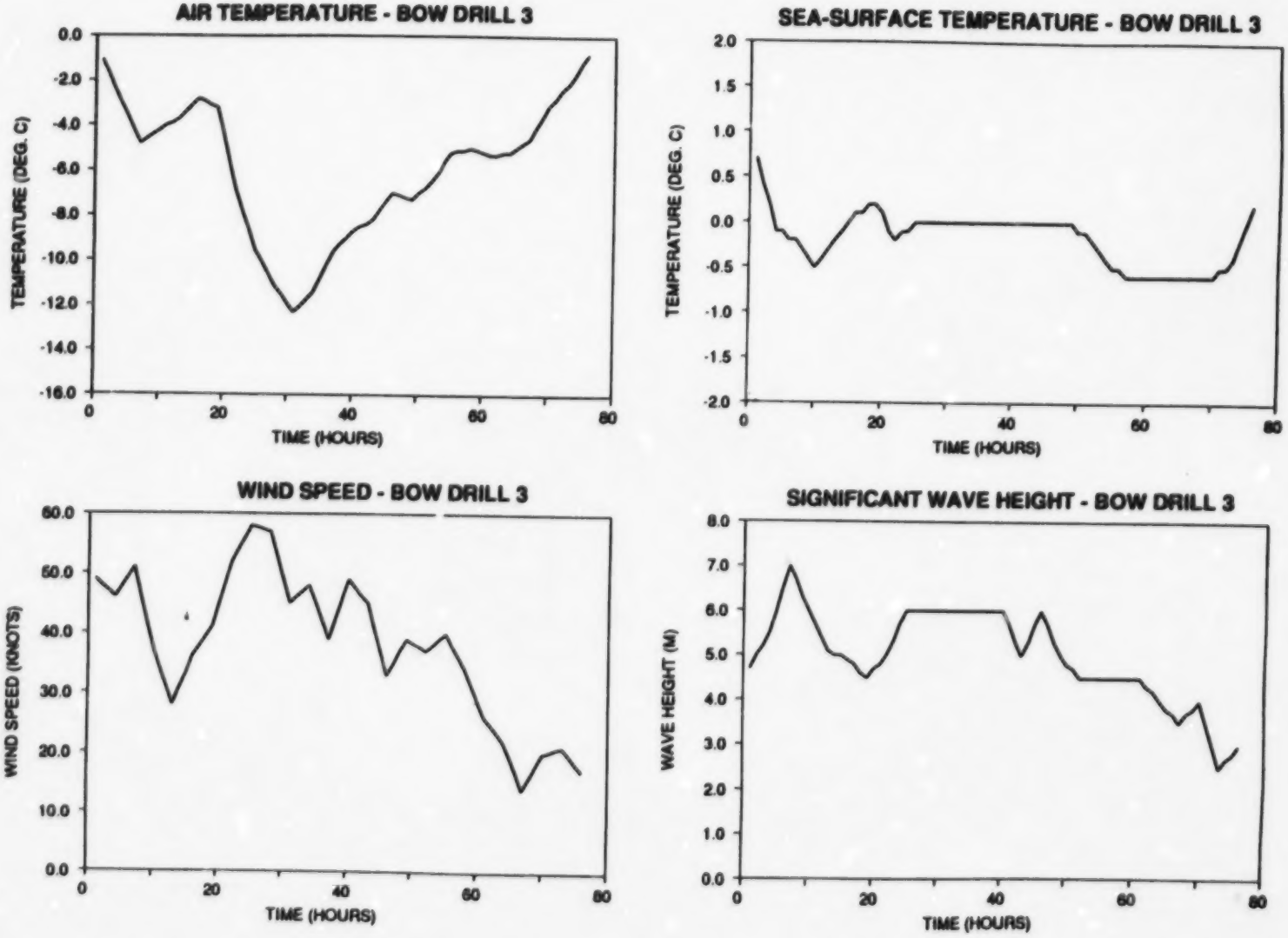


**Figure 4.16:** Meteorological and oceanographic conditions during the BOW DRILL 3 icing event.

GORILLA I was operating on the Scotian Shelf at 43.9°N, 60.6°W. Conditions conducive to icing lasted for two days. However most of the icing occurred during the first 9 hours of the event. Complete documentation of the event was not possible because the weather observer arrived after icing had begun. However, a series of photographs were taken at 1800 GMT on the 19th which were used to estimate the vertical ice thickness distribution on a vertical pipe (diameter = 0.46 meters). No ice mass estimates were available for the event. Hourly environmental data were obtained from the observer's log for all parameters except sea-surface temperature which was measured every 3 hours. A typical sea-surface salinity of 34 °/oo was assumed. Plots of the hourly model input data up till 1800 GMT on the 19th are shown in Figure 4.17. The models were run with this data, and vertical ice thickness profiles compared with the estimated profile obtained from the photographs.

OCEAN BOUNTY "A", December 17-24, 1979.

This event resulted in the largest documented accreted ice load on a semi-submersible. The event, documented in Nauman (1984), took place while the semi-submersible OCEAN BOUNTY was drilling in Lower Cook Inlet Alaska (59.0°N, 152.5°W). Conditions conducive to icing persisted for 7 days, with air temperatures of -14.0°C and wind speeds in excess of 80 knots during the period of maximum accretion (Fig. 4.18). In spite of the severity of this event, there is relatively little documentation available. The total ice accretion load is estimated to be 508 tonnes based on ballast records (Nauman and Tyagi, 1985). No thickness estimates are available although photos of the OCEAN BOUNTY show ice accretion in the order of a metre thick on the sides of the main deck and Nauman (1984) indicated that ice extended up to 30 mASL.

The weather reporting program on the OCEAN BOUNTY recorded the main icing parameters every 2 hours from 0600-1800 LST, with two additional wind speed reports at 0200 and 2200. This required the interpolation of much of the model input data over 12 hour periods each day. The interpolation is not considered to have introduced significant error into the icing model simulations because of the

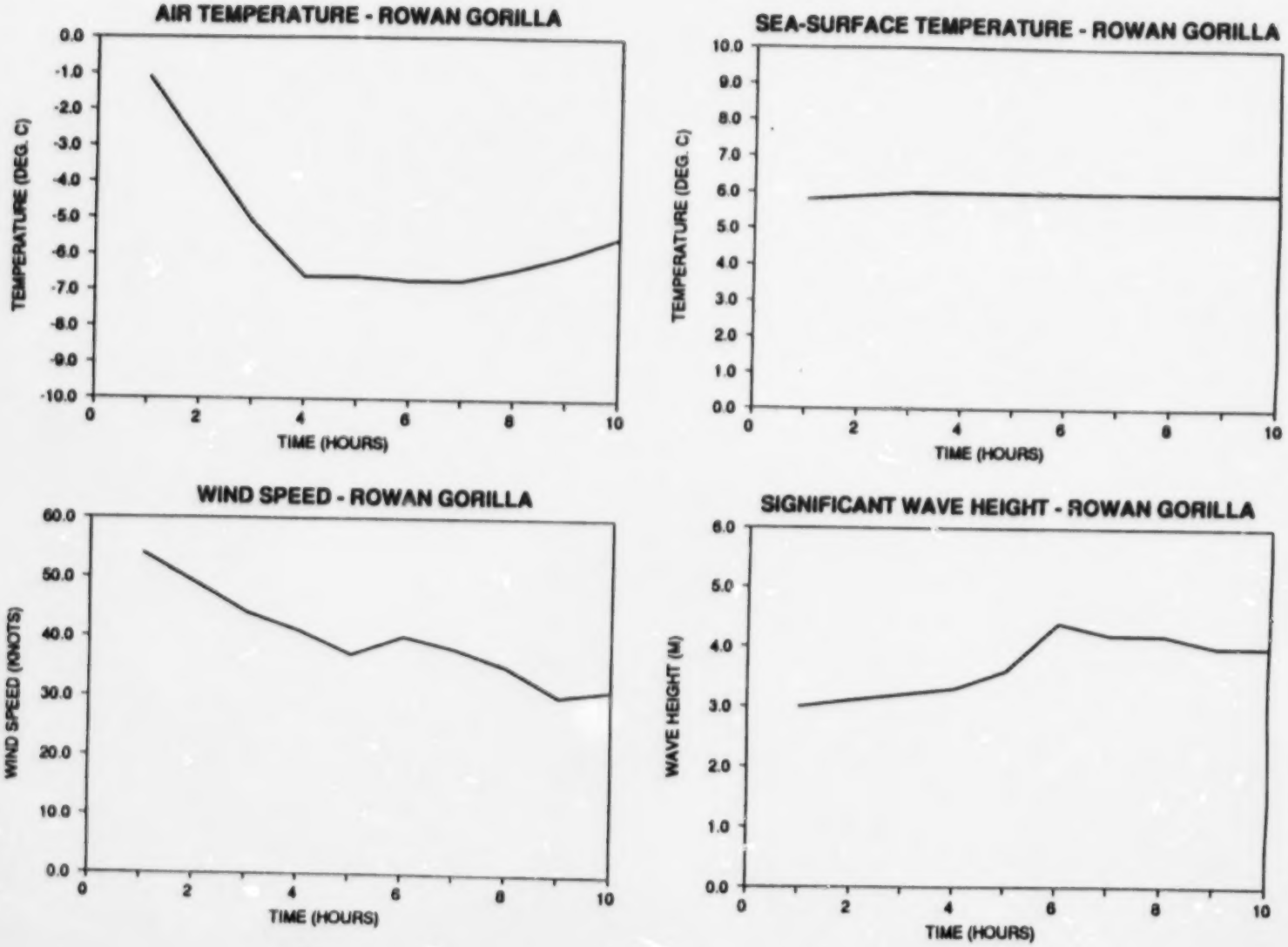


**Figure 4.17:** Meteorological and oceanographic conditions during the ROWAN GORILLA icing event.

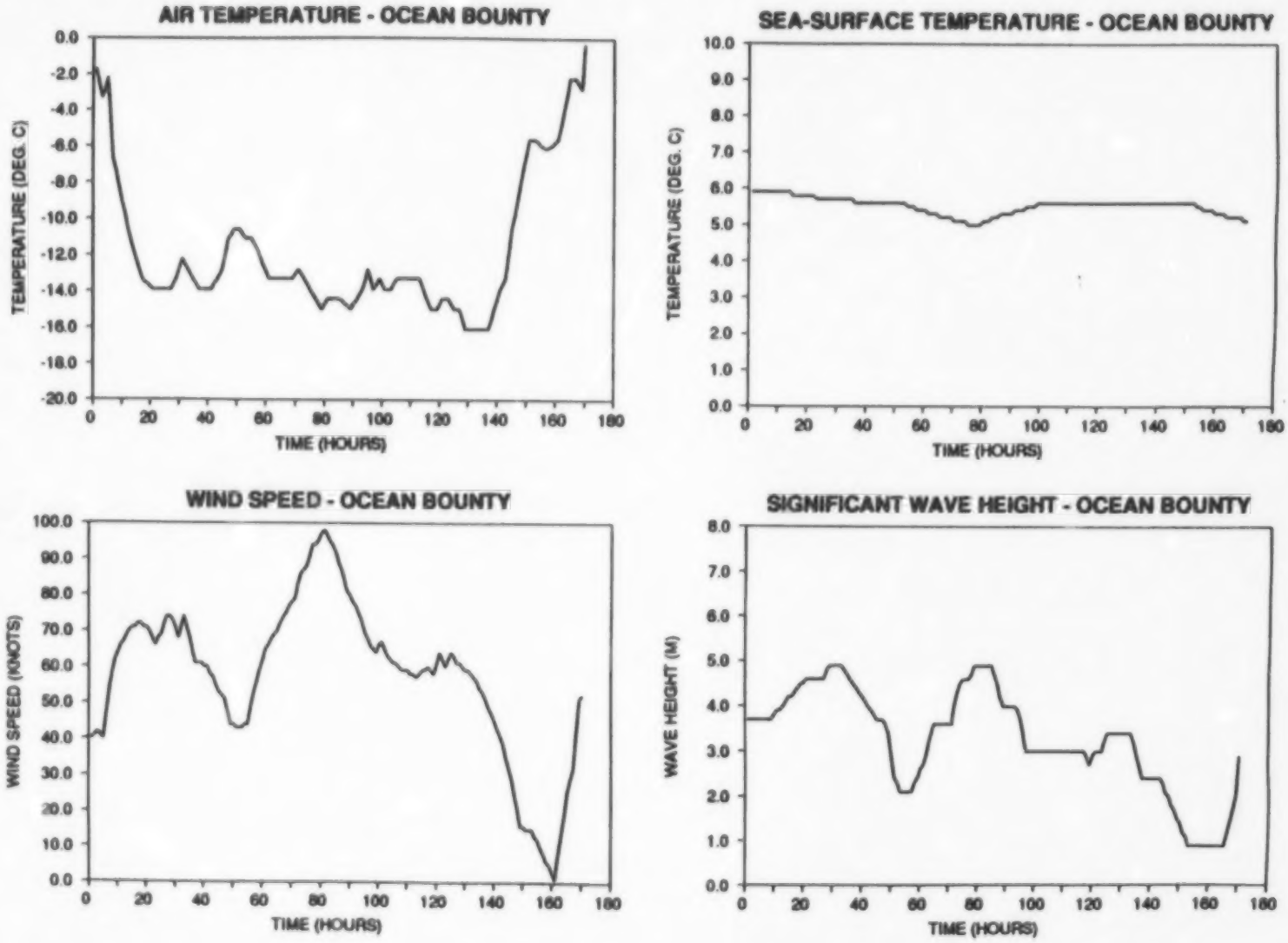


**Figure 4.18:** Meteorological and oceanographic conditions during the OCEAN BOUNTY icing event.

length of the event, and the relatively slow changing nature of conditions in Lower Cook Inlet during strong outflow events. Relative humidity was assumed to be 85% during the event (dewpoint temperatures were not measured) and sea-surface salinity was taken to be 32 °/oo based on the Soviet World Ocean Atlas. The models were run with the entire period of data for this event, and the total loads compared with the estimate provided by Nauman.

The above seven events yielded three rig icing cases where detailed vertical ice thickness information was available, and six cases with load estimates. The results of the model comparisons are presented below:

4.3.1 Ice thickness profiles

Detailed comparisons of observed and modelled vertical ice thickness distributions were possible for the SEDCO 708, SEDCO 709 and ROWAN GORILLA icing events. Figures 4.19 and 4.20 show modelled vertical ice thickness distributions and the corresponding profiles estimated from photos. For the diagonal member comparison, ICEMOD used the actual member inclination angle of 60°. RIGICE assumes a fixed 45° angle for inclined members.

Given that the accuracy of the thickness estimates is not likely to be better than ±50% and the accuracy in elevation is around ± 1 metre, both models provided quite reasonable results for the SEDCO 709 and ROWAN GORILLA profiles. However, both model predictions for the SEDCO 708 were poor, particularly for the diagonal truss. Part of this poor performance is very likely due to icicle formation processes which are not included in either model. RIGICE performed better at predicting the maximum ice thickness for the SEDCO 708 vertical column, however, the profile shape predicted by ICEMOD was more consistent with what was observed.

It is difficult to reach any firm conclusions about model performance from these few ice profiles. Taking into account the uncertainties in the ice data, both models appear to be capable of providing reasonable estimates of maximum ice accretion thickness on offshore structures. However, the vertical ice thickness

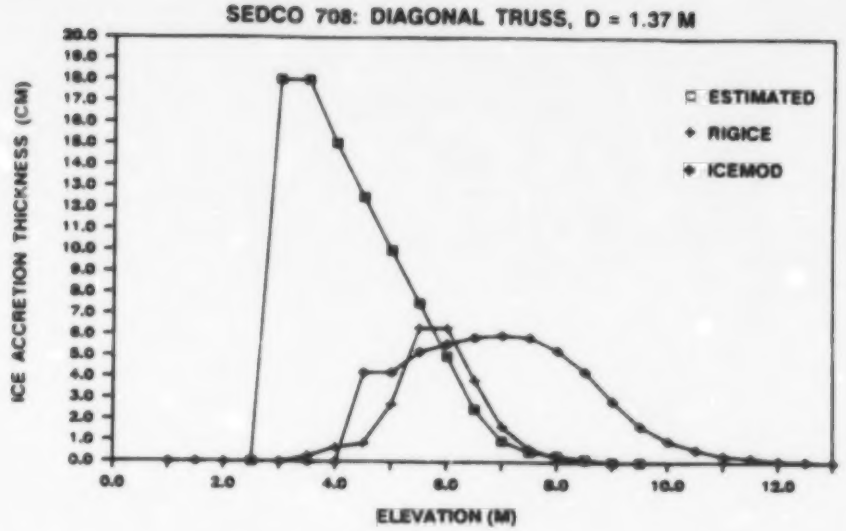


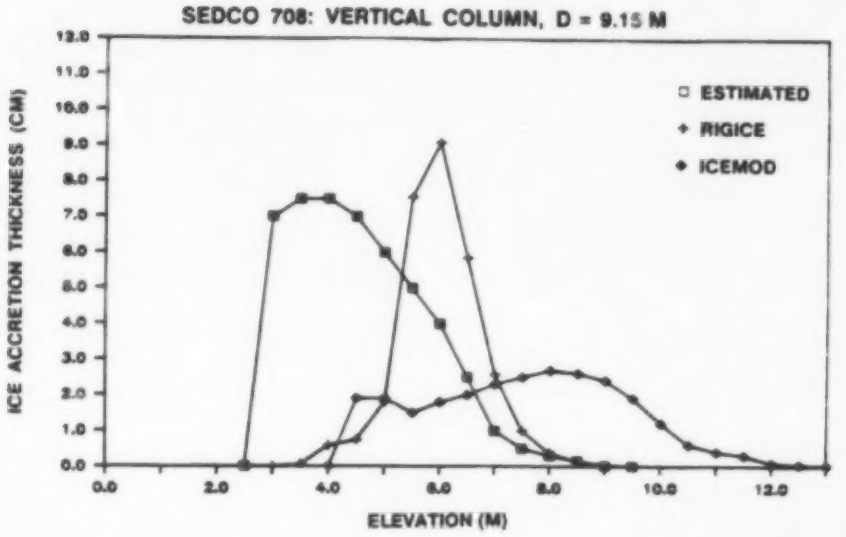


Figure 4.19: Comparison of ICEMOD and RIGICE modelled ice thickness profiles with profiles obtained by scaling photos.

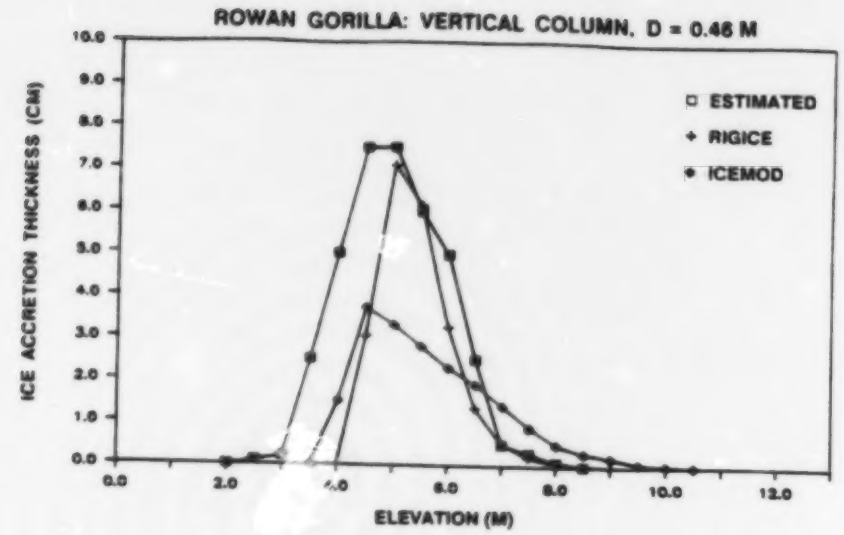


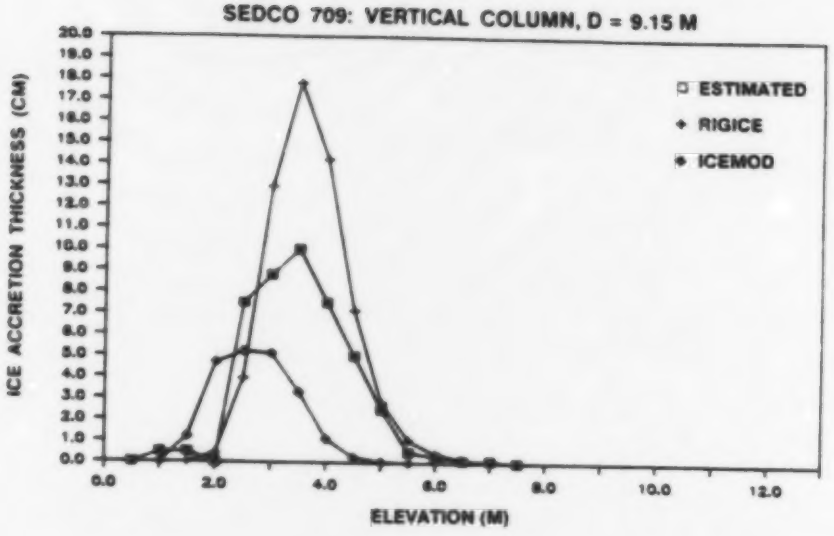


Figure 4.20: Comparison of ICEMOD and RIGICE modelled ice thickness profiles with profiles obtained by scaling photos.

distribution is not simulated as well. This is not surprising as the models contain very limited information about droplets and their movement in the turbulent air flow around a drilling platform. Another observation which can be made from the thickness profile comparison is that model performance appears to be inversely proportional to icing duration (9 hours for ROWAN GORILLA, 37 for SEDCO 709, and 60 for SEDCO 708). This is also not surprising since the longer the event, the greater the probability of encountering variables that are not taken into account or are poorly handled by the models.

4.3.2 Ice thickness observations

In addition to the above ice thickness profiles obtained from photographs, data such as maximum thickness and maximum vertical extent of accreted ice were also available from ice observer's logs. Maximum ice thickness, the elevation of the maxima and the maximum height of accreted ice are summarized in Table 4.4 together with the corresponding model predictions.

In spite of the obvious scatter evident in Table 4.4, a number of features can be seen. First, RIGICE performed very well at predicting the maximum vertical extent of accreted ice in all cases except the OCEAN BOUNTY. ICEMOD showed a tendency to overpredict the maximum accretion elevation. However, on the basis of the OCEAN BOUNTY results, ICEMOD may be more reliable for extreme conditions. The ability to predict the maximum height of accreted ice is important for safety and operational considerations e.g. to determine whether anti-icing strategies need to be employed to protect sensitive equipment.

When all 6 cases with thickness data are considered, ICEMOD provided more realistic maximum ice thicknesses. RIGICE tended to overpredict maximum ice thickness, particularly for large columns. Available evidence and experience shows that diagonal supports have thicker ice accretions than vertical columns because of accumulation and rundown of brine along the underside of the trusses. This phenomenon is correctly replicated by ICEMOD which includes brine film velocity in the icing equations. This process

Table 4.4

Comparison of observed and predicted ice accretion thickness data.

| Icing Event | Large Columns | | | Diagonal | | |
|---|---|---|---|---|---|---|
| | RIGICE | ICEMOD | Obs. | RIGICE | ICEMOD | Obs. |
| SEDCO 708 | | | | | | |
| max. thick (cm) | 9.0 | 2.7 | 7.5 | 6.3 | 6.1 | 18.0 |
| elevation (m) | 6.0 | 8.00* | 4.5 | 6.0 | 7.00* | 3.5 |
| max. height (m) | 9.0 | 13.00* | 9.0 | 9.0 | 13.00* | 9.0 |
| SEDCO 709 | | | | | | |
| max. thick (cm) | 17.8 | 5.3 | 10.0 | 12.5 | 11.8 | 15.0 |
| elevation (m) | 3.5 | 2.75 | 3.5 | 3.5 | 1.00 | 2.0 |
| max. height (m) | 7.0 | 5.00 | 7.0 | 7.0 | 4.50 | 7.0 |
| SEDCO 710 | | | | | | |
| max. thick (cm) | 33.6 | 11.1 | 10.0 | 24.2 | 24.1 | - |
| elevation (m) | 5.5 | 7.00* | - | 5.5 | 3.75* | - |
| max. height (m) | 9.5 | 13.00* | 9.0 | 9.5 | 13.00* | - |
| ROWAN GORILLA | | | | | | |
| max. thick (cm) | 7.1 | 3.9 | 7.5 | - | - | - |
| elevation (m) | 5.0 | 2.25 | 5.0 | - | - | - |
| max. height (m) | 8.5 | 10.00 | 8.0 | - | - | - |
| BOW DRILL 1 | | | | | | |
| max. thick (cm) | 37.8 | 11.0 | 5.0 | 27.9 | 23.3 | - |
| elevation (m) | 6.0 | 7.50* | - | 6.0 | 3.50* | - |
| max. height (m) | 9.5 | 15.00* | 7.0 | 9.5 | 15.00* | - |
| BOW DRILL 3 | | | | | | |
| max. thick (cm) | 47.1 | 12.2 | 7.5 | 35.6 | 25.6 | 15.0 |
| elevation (m) | 6.0 | 7.50* | - | 6.0 | 3.50* | - |
| max. height (m) | 9.5 | 15.00* | 12.0 | 9.5 | 15.00* | 12.0 |
| OCEAN BOUNTY | | | | | | |
| max. height (m) | 9.0 | 17.4* | 30.0 | - | - | - |

* Predicted ice would have exceeded this height - truncated by maximum elevation of structure modelled.

is not included in RIGICE and as a result, it predicts less ice on diagonals than large columns. The available evidence also indicates that the elevation of maximum ice thickness is lower on diagonals than vertical members which is also correctly replicated by ICEMOD.

### 4.3.3 Ice mass estimates

Table 4.5 presents results of the total ice mass comparison. To obtain some idea of the reliability of the estimated ice accretion loads reported by the observers, ice loads were also estimated based on available ice thickness information. The vertical profile obtained from photographs was used for the SEDCO 709, while an assumed vertical ice thickness distribution was used for the SEDCO 710, BOW DRILL 1 and BOW DRILL 3 events. Loads were computed assuming the same ice accretion profile applied to all members, ice accreted uniformly around a member, and ice density was 950 $kg/m^3$. These load estimates from thickness profiles are likely to be overestimates since sheltering effects were not considered. In light of this, the observer estimates are not unrealistic.

RIGICE results are presented for the average LWC configuration and a peak LWC formulation which used the same spray duration and spray frequency assumptions as ICEMOD. In addition, a simple post-processor program was used to incorporate sheltering effects into the average LWC version of RIGICE (figures in parentheses) because the model assumes ice accretes uniformly over all rig surfaces. The program derived a weighting factor for each structural element based on its accumulated icing index (the product of wind speed and absolute air temperature values < $-1.8^{\circ}C$) which takes into account the exposure of the element and wind direction. Corner columns were assumed to have an exposure range of $270^{\circ}$, while middle columns and diagonal trusses had an assumed exposure range of $180^{\circ}$. This scheme ensured that columns exposed during the maximum period of icing had the highest weighting factors.

Table 4.5 shows that the average LWC configuration of RIGICE provided reasonable ice load estimates for the OCEAN BOUNTY, SEDCO

708 and 709 events. However, it greatly overpredicted the SEDCO 710, BOW DRILL 1 and BOW DRILL 3 events, even when sheltering effects were included. The peak LWC configuration greatly underpredicted all six events and in spite of its more promising performance in the wind tunnel, appears to be an unacceptable configuration for reliable ice accretion load estimates on offshore structures. An attempt to "calibrate" this configuration with eqn. (4.3) did little to improve model results.

Table 4.5

Modelled and measured total accreted ice mass (tonne)

| Event | Observed | Est. | RIGICE avg. | RIGICE peak | ICEMOD |
|---|---|---|---|---|---|
| SEDCO 708 | 27.0[1] | - | 26.0 ( 17.4) | 2.9 | 21.4 |
| SEDCO 709 | 31.0[2] | 45.6[3] | 55.9 ( 36.6) | 12.0 | 17.5 |
| SEDCO 710 | 52.0[2] | 63.0[4] | 157.9 (123.1) | 19.4 | 115.4 |
| OCEAN BOUNTY | 508.0[5] | - | 409.1 (252.7) | 72.3 | 299.0 |
| BOW DRILL 1 | 10.0[2] | 17.0[4] | 94.7 ( 73.1) | 8.2 | 75.5 |
| BOW DRILL 3 | 20.0[2] | 39.0[4] | 137.0 ( 82.0) | 14.8 | 87.7 |

1. Obtained by Minsk from photographs
2. Estimated by ice observer from look-up table
3. Estimated from ice thickness profile
4. Estimated from assumed ice thickness profile
5. Estimated from ballast records, Mauman and Tyagi (1988)

ICEMOD also provided reasonable load predictions for the SEDCO 708, SEDCO 709 and OCEAN BOUNTY events. However, it too overpredicted the remaining three events, though by somewhat lesser amounts than RIGICE. When sheltering effects were included in RIGICE, the two models provided very similar load estimates: a linear regression analysis of RIGICE and ICEMOD total ice loads yielded an $r^2$ value of 0.98 and a slope of 0.81.

It was interesting to note that both models overpredicted the three events with the coldest average sea-surface temperatures and highest wave heights (see Table 4.3), and that all three events came from the Grand Banks. RIGICE response to cold sea-surface temperatures observed in the sensitivity analysis may contribute to the overprediction. However, this does not explain why ICEMOD

would overpredict the same events given its demonstrated insensitivity to sea-surface temperature. From information presented in Table 4.4 for the three events, it appears that a contributing factor to the ICEMOD overprediction is the accretion of ice over a much greater vertical extent than was experienced. The effect of this can be seen in Figure 4.21 which presents the vertical ice thickness distribution from ICEMOD for the windward side of a large column from the SEDCO 710 icing event. The reported maximum height of accreted ice for this event was 9.0 m. If the modelled profile is "compressed" to reflect this reported maximum height, the modelled ice load would be reduced by a factor of about 2, which is about the same magnitude that ICEMOD overpredicted total ice load for this event.

These results suggest that the empirical impact-generated spray expression or droplet trajectory assumptions used in ICEMOD are producing larger liquid water contents at higher elevations than are being experienced on the Grand Banks. The available evidence from icing events off the east coast of Canada is that the vertical extent of accreted ice occupies a relatively narrow band of about 6 m vertical extent, which moves up or down depending on the sea state. The vertical liquid water content profile will depend on wave height, wave period and wind speed, as well as platform characteristics (e.g. column diameter). Equation (2.30) indicates that ICEMOD only incorporates wind speed and wave height variation, which may explain the differences for the Grand Banks events. This highlights the necessity to develop and verify a theoretical approach to modelling the spray flux on vertical columns.

There are a number of reasons, in addition to those referred to above, which could account for the models overpredicting ice accretion loads. First, neither model is able to take into account the flow distortion in the wind field around a drilling platform which will have significant consequences for droplet transport and heat transfer at locations other than exposed windward structural elements. Second, neither model handles the complex spray generation process with any degree of sophistication. Third,

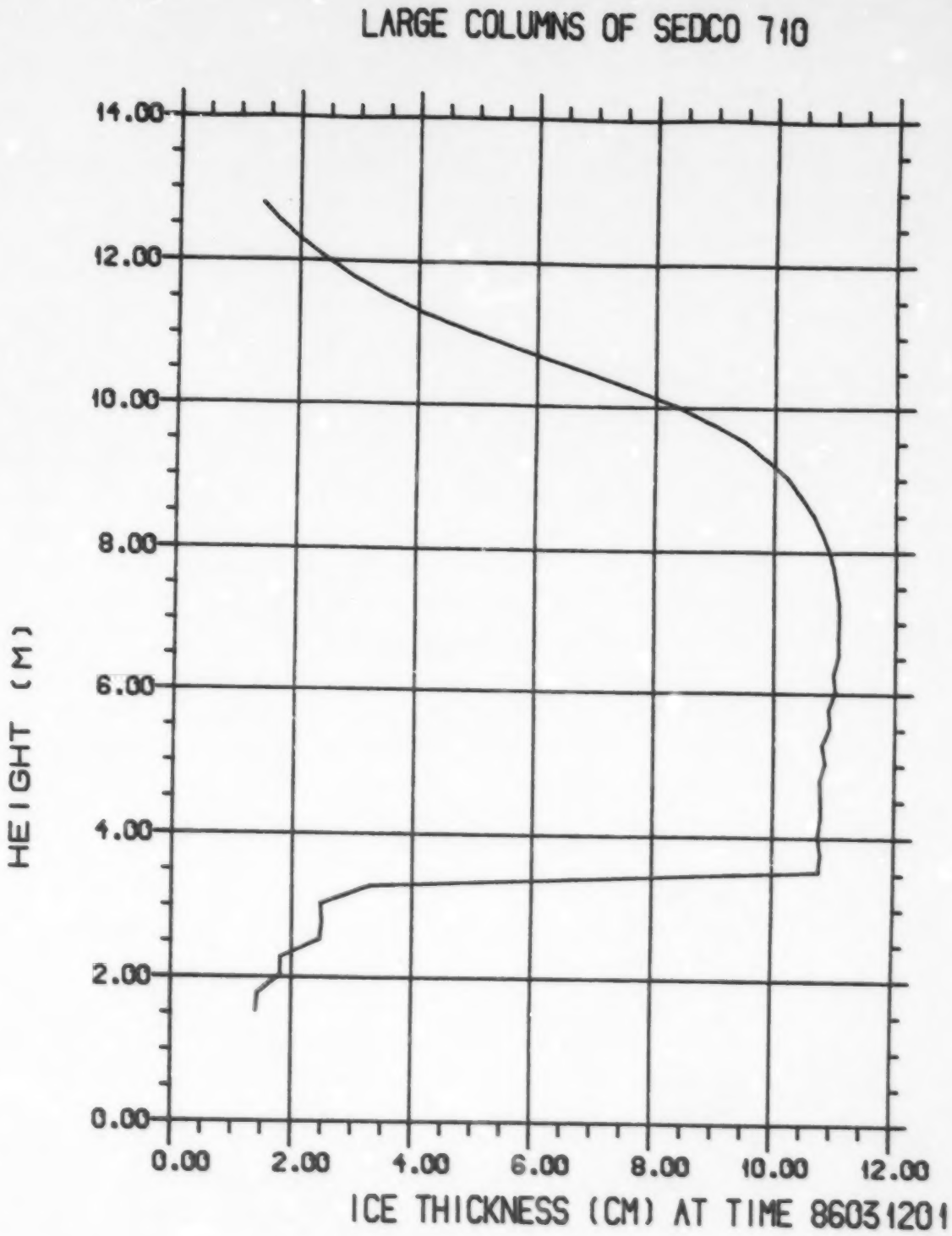


Figure 4:21: Vertical profile of ice thickness on the windward side of a large column as modelled by ICEMOD.

shedding of accreted ice from wave erosion and impact forces is not addressed by either model: this is likely to become important under high wave icing events. Finally, many of the mechanisms of time-dependent saline icing on vertical or inclined surfaces are just plainly unknown e.g. how the ice roughness and the local wind flow affects brine film movement. Ideally, these processes could be investigated under experimental conditions. However, this is complicated by the difficulty of simulating realistic marine icing conditions (high liquid water contents and saline water) in wind tunnels.

## 5.0 CONCLUSIONS

The main study conclusions are summarized below:

(1) Sensitivity analysis of a time-dependent and stationary drilling platform icing model showed similar model response to variation in the main icing parameters where sea surface temperatures were ~4.0°C. However, the stationary model exhibited greater sensitivity to a number of icing parameters when sea-surface temperatures were colder (~0.0°). The main reasons for the different stationary model response were considered to be related to a constant $\dot{Q}_w$ and the lack of the time-dependent feedback mechanism of increasing brine film salinity.

(2) Under fixed, pulsed spray conditions, the time-dependent model showed superior performance at predicting experimental ice loads in a wind tunnel environment. The average LWC configuration of RIGICE overpredicted ice loads while the peak LWC configuration underpredicted ice loads. This demonstrated the importance of understanding the physics of both in-spray and between-spray icing processes.

(3) In the wind tunnel, the peak LWC configuration of RIGICE was found to display essentially the same model response as ICEMOD, suggesting that some form of simple calibration may be possible to account for between-spray effects. However, this version was later found to greatly underpredict drilling

platform icing events. The encouraging wind tunnel performance displayed by this configuration was considered to be the result of the uniform test conditions employed.

(4) Both models provided good predictions of platform icing events for warmer water, low wave height icing conditions. However, both models were observed to overpredict icing for the cold water and higher wave height conditions typical of icing events on the Grand Banks. For RIGICE, the overprediction can be attributed in part to not including time-dependent effects. For ICEMOD, the evidence indicated the model was accreting ice at higher elevations than was reported. The reasons for this are uncertain, but may be related to the spray flux expressions or droplet flight assumptions used in ICEMOD.

## 6.0 RECOMMENDATIONS

The model comparisons carried out in this project have provided valuable insights into the importance of time-dependencies in the icing process, as well as give some idea of the performance of state-of-the-art marine icing models under both controlled and field conditions. However, further comparison of icing models along the lines of this study is unlikely to increase knowledge of the icing process, particularly where major portions of the models are empirically-based "black boxes", and when the accuracy of available icing data is low. The following areas need to be addressed in order to enhance our understanding of the icing process on offshore structures:

(i) There is an urgent need to develop a theoretical approach for modelling spray on offshore structures. This effort should go hand-in-hand with the collection of field data for model verification purposes.

(ii) Further evaluation of model performance in the field should only be carried out with measured icing data. This requires the development of a system which can

automatically monitor ice growth, yet resist the rigours of the spray zone. Ultra-sound sensors currently used in detecting airfoil icing (Hansman et al., 1988) show some promise.

(iii) Documentation of the nature and magnitude of time-dependencies in saline spray icing is required from wind tunnel experiments which closely approximate offshore icing conditions. The use of vertical wind tunnels such as the one recently constructed at the University of Alberta (Foy et al., 1987) will make this possible.

(iv) There is theoretical evidence (Horjen, pers. comm.) that accretion involving both spray and snow can considerably enhance ice loads. For example, a spray/snow version of ICEMOD used for a wind tunnel simulation accreted 77% more ice with a snowfall intensity corresponding to a visibility of 1.5 km. This process is particularly important during polar lows, but requires further verification.

The first three recommendations are currently being addressed in a coordinated effort by several government agencies including the Atmospheric Environment Service, Canada National Research Council (Institute for Marine Dynamics) and the U.S. Army Cold Regions Research and Engineering Laboratory.

## 7.0 REFERENCES


Agnew, T., 1985: The SEDNETH II[1] - a severe rig icing event on the east coast. Proc. Int'l. Workshop on Offshore Winds and Icing (T.A. Agnew and V.R. Swail eds.), Halifax, Nova Scotia, October 7-11, 1985, p. 388.

Achenbach, E.G., 1974: Heat transfer from smooth and rough surfaced circular cylinders in a cross flow. Proc. of the 5th Int'l. Heat Transfer Conference, Tokyo, p. 229-233.

Achenbach, E.G., 1977: The effect of surface roughness on the heat transfer from a circular cylinder to the cross flow of air. J. of Heat and Mass Transfer, 20:359-369.

Assur, A., 1958: Composition of sea ice and its tensile strength. In Arctic Sea Ice, U.S. National Academy of Sciences - National Research Council Pub. 598, pp. 106-138.

Brown, R.D. and P. Roebber, 1985: The ice accretion problem in Canadian waters related to offshore energy and transportation. Canadian Climate Centre Report 85-13, Atmospheric Environment Service, Downsview, Ontario, 295 pp.

Brown, R.D. and P. Mitten, 1988: Ice accretion on drilling platforms off the east coast of Canada. Paper presented at POLARTECH'88, Norwegian Institute of Technology, Trondheim, Norway, June 15-17, 1988.

Carstens, T., T.S. Jørgensen, T. Karterud and O. Skaret, 1984: The VHL sea spray icing tunnel. Proc. 2nd. Int'l. Workshop on Atmospheric Icing of Structures, Trondheim, Norway, June 19-21, 1984, p. 81-87.

Cox, G.F.N. and W.F. Weeks, 1986: Changes in the salinity and porosity of sea-ice samples during shipping and storage. J. Glaciology 32(112):371-375.

Foy, C.E., E.M. Gates and E.P. Lozowski, 1987: Design, instrumentation and performance of a refrigerated marine wind icing tunnel. Proceedings, 1987 Int'l. Symposium on Cold Regions Heat Transfer, Edmonton, Alberta, Canada, June 4-6, 1987, p. 137-142.

Gates, E.M., R. Narten, E.P. Lozowski and L. Makkonen, 1986: Marine icing and spongy ice. Proceedings of IAHR Ice Symposium, Iowa City, Iowa, p. 153-163.


[1] Should be SEDNETH I not SEDNETH II

Hansman, R.J., M.S. Kirby and F. Lichtenfelts, 1988: Ultrasonic techniques for aircraft ice accretion measurement. Preprint AIAA-88-4656-CP, AIAA/NASA/AFWAL Conference on Sensors and Measurement Techniques for Aeronautical Applications, 11 pp.

Horjen, I., 1981: Ice accretion on ships and marine structures. Marine Structures and Ships in Ice (MSSI) Report No. 81-02, 119 pp.

Horjen, I. and S. Vefsnmo, 1984a: Offshore Icing - Phase II - Extended theory of sea spray icing. OTTER Report, STF88 F83050, 100 pp.

Horjen, I. and S. Vefsnmo, 1984b: Mobile Platform Stability (MOPS) Subproject 02 - Icing (MOPS Report No. 15). NHL Report STF60 A284002, 56 pp.

Horjen, I. and S. Vefsnmo, 1985a: A kinematic and thermodynamic analysis of sea spray. Offshore Icing - Phase II, NHL-Report STF60 F85014 (in Norwegian).

Horjen, I. and S. Vefsnmo, 1985b: A numerical sea spray icing model including the effect of a moving water film. Proc. Int'l. Workshop on Offshore Winds and Icing (T.A. Agnew and V.R. Swail eds.), Halifax, Nova Scotia, October 7-11, 1985, p. 152-164.

Horjen, I. and S. Vefsnmo, 1986a: Computer modelling of sea spray icing on marine structures. Automation for Safety in Shipping and Offshore Operations (ASSOPO) (G. Kuo et al., eds.), Elsevier Science Publishers B.V. (North-Holland).

Horjen, I. and S. Vefsnmo, 1986b: Calibration of ICEMOD - Extension to a time dependent model. NHL-Report, STF60 F86040, April -86, 68 pp.

Horjen, I. and S. Vefsnmo, 1987: Time-dependent sea spray icing on ships and drilling rigs - a theoretical analysis. NHL-report STF60 F87130, November 1987, 87 pp.

Horjen, I., S. Vefsnmo and P.L. Bjerke, 1988: Sea spray icing on rigs and supply vessels. ESARC Report No. 15, STF60 F88137, 98 pp.

Jørgensen, T.S., 1982: Influence of ice accretion on activity in the northern part of the Norwegian Continental Shelf. OTTER Report STF88 F82016, 142 pp.

Jørgensen, T.S., S. Vefsnmo and I. Horjen, 1986: Offshore icing - Phase II. Final Report. NHL-report STF60 F 86084, 34 pp.

Landau and Lifschitz, 1959: Fluid mechanics. Pergamon Press, 1959.

Løset, S. and S. Vefsnmo, 1986: Computer modelling of ice accretion and control of icing on marine units. POLARTECH'86, Int'l. Offshore and Navigation Conf. and Exhibition, Finland, Oct., 1986.

Lozowski, E.P , J.R. Stallabrass and P.F. Hearty, 1979: The icing of an unheated non-rotating cylinder in liquid water droplet-ice crystal clouds. Mech. Eng. Report LTR-LT-96, Nat. Res. Council, Canada, 109 pp.

MacLaren Plansearch, 1986: Final report of the offshore icing measurement project, Scotian Shelf, 1986. Contractors final report prepared for Atmospheric Environment Service, Bedford, Nova Scotia.

Makkonen, L., 1985a: Heat transfer and icing of a rough cylinder. Cold Regions Sci. and Tech. 10:105-116.

Makkonen, L., 1985b: Icing rates on cylindrical structures. Proc. Int'l. Workshop on Offshore Winds and Icing (T.A. Agnew and V.R. Swail eds.), Halifax, Nova Scotia, October 7-11, 1985, p. 140-151.

Minsk, L.D., 1984: Ice observation program on the semisubmersible drilling vessel SEDCO 708. CRREL Special Report 84-2, 14 pp.

Narten, R., E.M. Gates and E.P. Lozowski, 1986: The influence of several factors on the heat transfer from an isothermal cylinder. Preprint from 3rd Int'l. Workshop on Atmospheric Icing of Structures, Vancouver, British Columbia, Canada, May 6-8, 1986.

Nauman, J.W., 1984: Superstructure icing on the semisubmersible OCEAN BOUNTY in Lower Cook Inlet, Alaska. Proc. 2nd. Int'l. Workshop on Atmospheric Icing of Structures, Trondheim, Norway, June 19-21, 1984, p. 71-79.

Nauman, J.W. and R. Tyagi, 1985: Superstructure icing and freezing conditions on offshore drill rigs, Alaska experience and regulatory implications. Proc. Int'l. Workshop on Offshore Winds and Icing (T.A. Agnew and V.R. Swail eds.), Halifax, Nova Scotia, October 7-11, 1985, p. 57-68.

Roebber, P. and P. Mitten, 1987: Modelling and measurement of icing in Canadian waters. Canadian Climate Centre Report 87-15, Atmospheric Environment Service, Downsview, Ontario, 150 pp.

Rohsenow, W.M. and Choi, H.Y., 1961: Heat, mass and momentum transfer. Prentice Hall, Inc., 1961.

Schlicting, H., 1955: Boundary layer theory. McGraw-Hill, First English edition, 535 pp.

Schlicting, H., 1979: Boundary layer theory. McGraw-Hill, Seventh English edition, 817 pp.

Smith, S.D., 1980: Wind stress and heat flux over the ocean in gale force winds. J of Phys. Ocean., Vol. 10, p. 709-726.

Stallabrass, J.R., 1980: Trawler icing. A compilation of work done at N.R.C. Mechanical Engineering Report MD-56, 101 pp.

Tabata, T, 1969: Studies of ice accumulation on ships, III. Low Temperature Science, Ser. A, pt. 27, p. 337-349 (in Japanese).

Vefsnmo, S., 1986: ICEMOD - analysis of icing on marine structures. User's manual. NHL Report STF60 F86033, April 1986, 36 pp.

Vefsnmo, S., I. Horjen and S. Løset, 1987: Time-dependent numerical model for sea spray icing on marine structures. Paper presented at 9th Int'l. Conference on Port and Ocean Engineering under Arctic Conditions (POAC), Fairbanks, Alaska, August 17-21, 1987.

Witting, R.L., 1908: A study of water level variations and water exchange in the Finnish sea areas. Finnlandische Hydrographisch-Biologische Untersuchungen, 2 (in German).

Wu, J., 1982: Sea spray: a further look. J.G.R. Vol. 87(C11), p. 8905-8912.

Wu, J., J.J. Murray and R.J. Lai, 1984: Production and distribution of sea spray. J.G.R., Vol. 89(C5), p. 8163-8169.

Zakrzewski, W.P., 1986: Icing of ships. Part I: Splashing a ship with spray. NOAA Technical Memorandum ERL PMEL-66, 74 pp.

# APPENDIX A:

## HEAT EXCHANGE RELATIONSHIPS USED IN "ICEMOD" FOR THE BRINE FILM

1. The convective heat flux, $\dot{Q}_c$:

Heat is convected away from the air boundary by free (thermal) convection and forced (external flow) convection. During sea spray icing, wind speeds are typically quite high which means that heat transfer from the icing surface by thermal convection is negligible compared to forced convective heat transfer. Hence, only the latter is considered. If $\beta$ is the heat transfer coefficient for forced convection then:

$$\dot{Q}_c = \beta (\theta_a - \theta_b) \tag{A1}$$

or in terms of the Nusselt number, Nu,

$$\dot{Q}_c = \frac{k_a}{L} Nu (\theta_a - \theta_b) \tag{A2}$$

The following expressions were obtained from the literature for local values of Nu for the three geometries considered in the text:

Horizontal plate

Assuming a turbulent air boundary layer, the local Nusselt number for a smooth plate is given by (Rohsenow and Choi, 1961):

$$Nu_x = 0.0296 \, Re_x^{0.8} \, Pr^{1/3} \tag{A3}$$

where the local Reynolds number is defined by

$$Re_x = \frac{Ux}{\nu} \tag{A4}$$

x = distance from leading edge

Vertical plate

The Nusselt number given by eqn. (A3) may also be used for this case if U is the local wind velocity above the air boundary layer, and x is the distance from the stagnation line.

Assuming a potential flow field:

$$U(x) = \frac{2U_0 x}{\sqrt{L^2 - x^2}} \qquad (A5)$$

where L = plate width

Horizontal or vertical cylinder

The experimental results of Achenbach (1977) for a cylinder with roughness parameter $k_s/D = 9 \cdot 10^{-3}$ shows that the local Nusselt number may be approximated by

$$Nu = Nu_0 \left[ 2 + \sin \left( \frac{18\varphi}{5} - \frac{\pi}{2} \right) \right], \quad -\frac{5\pi}{9} \leq \varphi \leq \frac{5\pi}{9} \qquad (A6)$$

$$Nu = Nu_0 \left[ 2 + \sin \left( \frac{9\varphi}{8} + \frac{7\pi}{8} \right) \right], \quad \frac{5\pi}{9} < \varphi \leq \pi \qquad (A7)$$

$$Nu = Nu_0 \left[ 2 + \sin \left( \frac{9\varphi}{8} - \frac{\pi}{8} \right) \right], \quad \pi < \varphi < \frac{13\pi}{9} \qquad (A8)$$

where $Nu_0$ is the Nusselt number at the front stagnation line, and $\varphi$ is the angle in radians from this line, positive clockwise. Note that these expressions fulfil the requirement of continuity around the entire cylinder circumference.

Equation (A6) has the same form as the empirical formula of Lozowski et al. (1979) based on some earlier experiments of Achenbach (1974) with $Re_0 = 2.6 \cdot 10^5$. The maximum value of the Nusselt number is obtained from $Nu = 3\ Nu_0$ at $\varphi = \pm 5\pi/18$ i.e. at $\pm 50^\circ$ from the front stagnation line. On the lee side of the stagnation line $Nu = 2\ Nu_0$ from equation (A7).

From a physical point of view, $Nu_0$ should be equal to the smooth cylinder value and hence proportional to the square root of the Reynolds number:

$$Nu_0 = g(I) \sqrt{Re} \qquad (A9)$$

where g(I) is some function of the free stream turbulence intensity, I. From Lozowski et al. (1979) g(I) = 1.2 which corresponds to a turbulence intensity of about 5% (Narten et al., 1986). This is a typical value for wind tunnels.

However, a least squares fit to experimental data for $\varphi = 5\pi/18$ and $\varphi = \pi$ yields

$$Nu_0 = 1.58 \cdot 10^{-2}\ Re^{0.338},\ \varphi = 0 \qquad (r^2 = 0.969) \qquad (A10)$$

If only data from the lee side stagnation line are used, the Nusselt number is approximated by

$$Nu = 2.32 \cdot 10^{-2}\ Re^{0.858},\ \varphi = \pi \qquad (r^2 = 0.974) \qquad (A11)$$

For this study, equations (A6) and (A9) were used to calculate icing on the front side of cylinders, while equation (A11) was used for the lee side.

2. The evaporative heat flux, $\dot{Q}_e$

From eqn. (2.5):

$$\dot{Q}_e = \beta \frac{\theta_{ev}}{p} [f\ e(\theta_a) - e_b(\theta_b, S_b)] \qquad (A12)$$

where

$$\theta_{ev} = 0.622 \frac{l_e}{Le\ C_a} \approx 1749^{\circ}C$$

3. Heat transfer between impinging spray and liquid brine film, $\dot{Q}_w$

Generally, the sensible heat exchange between a droplet cloud and a wet surface kept at an equilibrium temperature $\theta_b$ is:

$$\dot{Q}_w = C_w \left[ \int_{d_1}^{d_2} \theta(x)\ d\eta_w(x) - R_w \theta_b(t) \right] \qquad (A13)$$

(Actually, the "equilibrium temperature" is a mathematical simplification - see Lozowski et al., 1979).

$\eta_w(x)$ is the water catch rate of droplets with diameter x, i.e. $\eta_w(x) = \gamma(x)\, u_0(x)\, M(x)$, where $u_0(x)$ is the free droplet velocity in the horizontal (wind) direction. Thus:

$$d\eta_w(x) = \eta_w(x) \left[ \frac{dM}{M(x)} + \frac{d\gamma}{\gamma(x)} + \frac{du_0}{u_0(x)} \right] \tag{A14}$$

or, for large droplets with a "long" flight time:

$$d\eta_w(x) \approx \eta_w(x) \frac{dM}{M(x)} = \frac{\gamma(x) u_0(x)}{\gamma_t U^0_{sp}} R_w f dx \tag{A15}$$

where $U^0_{sp}$ is the free flow spray bulk velocity. Introducing the last expression in eqn. (A13) gives:

$$\dot{Q}_w = C_w R_w \left[ \frac{1}{\gamma_t U^0_{sp}} \int_{d_1}^{d_2} \gamma(x)\theta(x) u_0(x) f(x) dx - \theta_b \right] \tag{A16}$$

where f(x) is the fractional volume of droplet diameter.

4. Heat transfer by radiation, $\dot{Q}_r$

Horjen (1981) approximated $\dot{Q}_r$ by:

$$\dot{Q}_r \approx \beta_r (\theta_a - \theta_b) \tag{A17}$$

where $\beta_r \approx 4.48$ W/m$^2$deg

5. Heating due to adiabatic compression and viscous work in the boundary layer, $\dot{Q}_v$

From Landau and Lifschitz, 1959:

$$\dot{Q}_v = \beta\eta \frac{U_0^2}{2C_a} \tag{A18}$$

where $\eta$ is the recovery factor. For a turbulent air boundary layer:

$$\eta = 1 - \left(\frac{U^2}{U_0}\right)\left(1 - Pr^{1/3}\right) \qquad \text{(A19)}$$

which gives

$$\eta = \begin{cases} 0.89 & , \quad \text{horizontal plate} \\ 0.95 & , \quad \text{vertical plate} \\ 1 - 0.43 \sin^2\varphi & , \quad \text{horizontal cylinder} \end{cases}$$

6. Conductive heat flow through the ice layer, $\dot{Q}_i$

$$\dot{Q}_i = - k_i \left.\frac{\partial \theta_i}{\partial n}\right|_{n=0} \qquad \text{(A20)}$$

Ice formed by sea spray is rather spongy. In ICEMOD, 66% of the ice mass near the icing surface is assumed to consist of pure ice while the rest is brine. The salinity of brine occlusions close to the surface is approximately equal to the brine film salinity. If chemical equilibrium exists between ice and brine, the temperature of the ice is more or less constant in a thin layer near the ice surface. The heat loss through the ice during spray icing is therefore rather small, and may be neglected. However, heat loss to the underlying structure may be important in the beginning of an icing event.